MECHANISMS GOVERNING NF-κB REGULATION BY THE ANTI-INFLAMMATORY PROTEIN A20

APPROVED BY SUPERVISORY COMMITTEE

Zhijian 'James' Chen, Ph.D.

Melanie Cobb, Ph.D.

Paul Sternweis, Ph.D.

Felix Yarovinsky, M.D.

Acknowledgements

I thank James Chen for his mentorship during my four years of graduate training. He encouraged me to work on a subject that is highly competitive and has already been published on extensively, with the premise that these publications left room for doubt, and applying his approach would lead to important insights. This premise proved to be correct. James' approach to science, including the types of questions to ask, the approaches to address them, the experimental rigor required to confidently draw conclusions, and the style of communicating his work to the field, is exemplary. As I have become more competent intellectually and experimentally, he has also shown great willingness to entertain my ideas and to allow me the time needed to test them. I have also co-authored two reviews and a meeting report with James, and have presented my work twice at excellent meetings. For these opportunities I am very grateful.

I also thank a few colleagues who have directly contributed to my work. Jueqi Chen performed a key experiment testing the ability of catalytically inactive A20 to impair IKK activation in vitro. She also found evidence that IKK activation by TAK1 is dependent on polyubiquitin chains, an idea that I built upon when characterizing the mechanism of IKK inhibition by A20. Lijun 'Josh' Sun and Zong-Ping Xia provided much-needed technical input. Lab manager Beethoven Ramirez made sure any reagent I needed was available. Fenghe Du assisted with cloning of some A20 constructs. Averil Ma (UCSF) provided $A20^{-/-}$ MEFs. Adrian Ting (Mount Sinai School of Medicine) provided retroviral constructs and protocol. Ye Zhang (UNC Chapel Hill) provided lentiviral constructs and protocol.

I also thank my family for supporting me even though they have trouble understanding the work I am doing and why I chose to pursue a PhD. Their patience and encouragement are a true blessing.

For 3 and ½ years of my time in the lab I was supported by an NIH pre-doctoral training grant (GM007062).

MECHANISMS GOVERNING NF-κB REGULATION BY THE ANTI-INFLAMMATORY PROTEIN A20

by

Brian Skaug

DISSERTATION

Presented to the Faculty of the Graduate School of Biomedical Sciences

The University of Texas Southwestern Medical Center at Dallas

In Partial Fulfillment of the Requirements

For the Degree of

DOCTOR OF PHILOSOPHY

The University of Texas Southwestern Medical Center at Dallas

Dallas, Texas

June 27th, 2011

MECHANISMS GOVERNING NF-κB REGULATION BY THE ANTI-INFLAMMATORY PROTEIN A20

Brian Skaug

The University of Texas Southwestern Medical Center at Dallas, 2011

Mentor: Zhijian 'James' Chen, Ph.D.

A20 is a potent anti-inflammatory protein that inhibits NF-κB, and A20 dysfunction is associated with autoimmunity and B-cell lymphoma. A20 harbors a deubiquitination enzyme domain and can employ multiple mechanisms to antagonize ubiquitination upstream of NEMO, a regulatory subunit of the IκB kinase complex (IKK). However, direct evidence of IKK inhibition by A20 is lacking, and the inhibitory mechanism remains poorly understood. Here we show that A20 can directly impair IKK activation without deubiquitination or impairment of ubiquitination enzymes. We find that polyubiquitin binding by A20, which is largely dependent on A20's seventh zinc finger motif (ZnF7), induces specific binding to NEMO. Remarkably, this ubiquitin-induced recruitment of A20 to NEMO is sufficient to block IKK phosphorylation by its upstream kinase TAK1. Our results suggest a novel mechanism of IKK inhibition and a means by which polyubiquitin chains can specify a signaling outcome.

Table of Contents

List of Publications

Skaug B, Chen J, Du F, Ma A, He J, Zhang Y, Chen ZJ. "Direct, non-catalytic mechanism of IKK inhibition by A20." revised for *Mol Cell.*

Hou F, Sun L, Zheng H, Skaug B, Jiang QX, Chen ZJ. "MAVS forms prion-like aggregates to activate and propagate antiviral innate immune response. *Cell*. In press.

Xu K, Sacharidou A, Fu S, Chong DC, Skaug B, Chen ZJ, Davis GE, Cleaver O. "Blood vessel tubulogenesis requires Rasip1 regulation of GTPase Signaling." *Dev Cell*. 2011 Apr 19;20(4):526-39

Skaug B, Chen ZJ. "Emerging role of ISG15 in antiviral immunity." *Cell.* 2010 Oct 15;143(2):187-90. Review.

Skaug B, Chen ZJ. "SUMO, Ubiquitin, UBL Proteins: Implications For Human Diseases-Fifth International Conference." *IDrugs.* 2010 Apr;13(4):224-7

Xu M, Skaug B, Zeng W, Chen ZJ. "A ubiquitin replacement strategy in human cells reveals distinct mechanisms of IKK activation by TNFalpha and IL-1beta." *Mol Cell.* 2009 Oct 23;36(2):302-14

Skaug B, Jiang X, Chen ZJ. "The role of ubiquitin in NF-κB regulatory pathways" *Ann Rev Biochem*. 2009;78:769-96. Review.

Upreti M, Lyle CS, Skaug B, Du L, Chambers TC. "Vinblastine-induced apoptosis is mediated by discrete alterations in subcellular location, oligomeric structure, and activation status of specific Bcl-2 family members" *J Biol Chem*. 2006 Jun 9;281(23):15941-50

List of Figures

List of Abbreviations

NF-κB	nuclear factor kappa-light-chain-enhancer of activated B cells
IκB	Inhibitor of NF-κB
IKK	IκB kinase
NEMO	NF-κB essential modulator
TNFα	Tumor necrosis factor alpha
IL-1β	Interleukin-1beta
TAK1	Transforming growth factor beta-activated kinase
TAB	TAK1-binding protein
RIP1	Receptor-interacting protein kinase 1
TRAF	TNF receptor-associated factor
TNFR	TNF receptor
IL-1R	Interleukin-1 receptor
TLR	Toll-like receptor
IL-6	Interleukin-6
COX-2	Cyclooxygenase-2
OTU	ovarian tumor domain
vOTU	OTU domain from the L1 protein from Crimean Congo Hemorrhagic Fever Virus
TAX1BP1	TAX1-binding protein
Ub	Ubiquitin
polyUb	Polyubiquitin chains

Introduction

NF-κB, a dimeric transcription factor consisting of the Rel family of proteins, controls genes involved in inflammation, immunity, and cell survival (Hayden and Ghosh, 2008). Under basal conditions, NF-κB is sequestered in the cytoplasm by inhibitor of NF-κB (IκB). Stimulation of cells with any of a multitude of agents, including inflammatory cytokines and toll-like receptor (TLR) ligands, induces IκB phosphorylation by the IκB kinase (IKK). Phosphorylated IκB is ubiquitinated, then degraded by the proteasome, liberating NF-κB to enter the nucleus and regulate gene expression (see Introductory Figure for diagram summarizing mechanisms of NF-κB regulation).

Ubiquitin also has non-degradative functions in the IKK-regulatory pathways (Chen and Sun, 2009). Indeed, binding of the TNF receptor (TNFR), IL-1 receptor (IL-1R), and many TLRs to their respective ligands results in activation of ubiquitin ligases. In the IL-1R and many TLR pathways, TNF receptor-associated factor 6 (TRAF6) is the major ubiquitin ligase. TRAF6 works with the dimeric ubiquitin-conjugating enzyme UBC13/UEV1A to synthesize polyubiquitin chains linked through Lys 63 of ubiquitin (K63) (Deng et al., 2000). Indeed, the E3 ligase activity of TRAF6, the catalytic activity of UBC13, and K63 of ubiquitin are required for IL-1β-induced IKK activation (Lamothe et al., 2008; Xu et al., 2009). In the TNFR pathway, numerous ubiquitin ligases are recruited, including TRAF2, cellular inibitor of apoptosis (cIAP) 1 and 2, and linear ubiquitin chain assembly complex (LUBAC) (Bianchi and Meier, 2009; Haas et al., 2009). The linkage of polyubiquitin chains in this pathway remains enigmatic, and it is unclear why so many ubiquitin ligases, and potentially different polyubiquitin linkages, are involved. Nevertheless, polyubiquitin chains clearly play an essential role in TNFα-induced IKK activation. In the TNFR pathway, receptor-interacting protein kinase 1 (RIP1) is a key ubiquitination substrate (Ea et al., 2006; Wu et al., 2006). In the IL-1R/TLR4 pathway, IL-1R

Introductory Figure

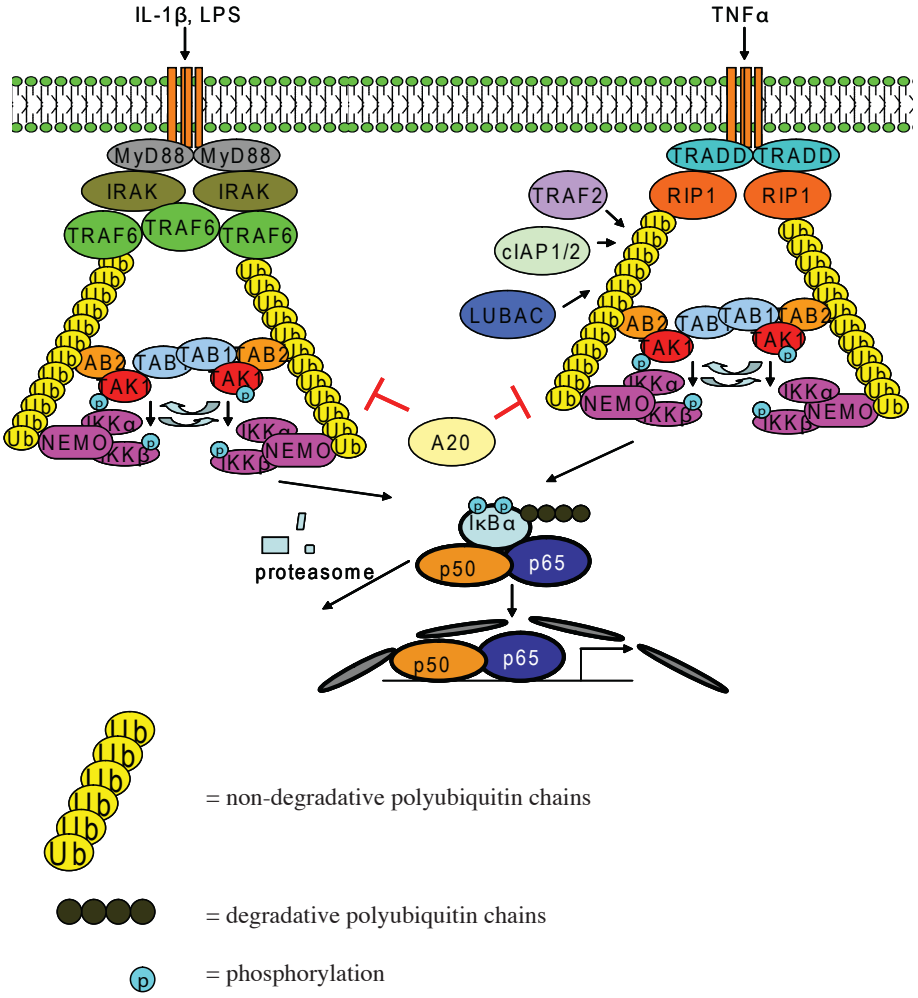

Figure 1.1. A model for regulation of NF-κB by IL-1β and TNFα.
Detection of IL-1β or TNFα results in the recruitment and activation of E3 ubiquitin ligases. In the IL-1R pathway, TRAF6 is the key E3 ligase. In the TNFR pathway, multiple E3 ligases including TRAF2, cIAP's 1/2, and LUBAC appear to be involved. The resulting polyubiquitin chains recruit and activate the TAK1 and IKK kinase complexes through ubiquitin binding to the regulatory subunits TAB2 and NEMO, respectively. Activated IKKβ phosphorylates IκBα, targeting it for ubiquitination and degradation by the proteasome. NF-κB, pictured here as the p50/p65 dimer, is then liberated to enter the nucleus, where it regulates genes involved in inflammation and cell survival. A20 is a potent negative regulator of NF-κB signaling, and A20 dysfunction is associated with autoimmunity and B-cell lymphoma.

associated kinase 1 (IRAK1) and TRAF6 are ubiquitination substrates, but only unanchored polyubiquitin chains synthesized by TRAF6 and UBC13/UEV1A have been demonstrated to directly activate TAK1 and IKK (Xia et al., 2009). The polyubiquitin chains in each pathway bind to the regulatory subunits of the TGFβ-activated kinase (TAK1) and IKK complexes, TAB2 and NEMO, respectively, and this binding leads to TAK1 and IKK activation (Ea et al., 2006; Kanayama et al., 2004; Laplantine et al., 2009; Wu et al., 2006). Activated TAK1 phosphorylates IKK, as well as the MAP kinase kinase MKK6, promoting activation of IKK and MAP kinase signaling pathways (Wang et al., 2001).

Whereas robust NF-κB activation is important for appropriate inflammatory and immune response to infection, excess NF-κB activity can lead to inflammatory disease (Hayden and Ghosh, 2008). In addition, excess NF-κB activity promotes tumorigenesis due to its upregulation of anti-apoptotic genes (Baud and Karin, 2009). Thus, negative regulation of NF-κB is essential for proper immune homeostasis and tumor suppression. A multitude of mechanisms are employed to ensure proper negative regulation of NF-κB, many of which rely on NF-κB-dependent transcription of negative-regulatory proteins (Hayden and Ghosh, 2008). IκB is one of the proteins upregulated by NF-κB, forming a simple negative feedback loop in which the new IκB population re-sequesters NF-κB in the cytoplasm. However, this mechanism must be coupled to downregulation of IKK activity, so that the new IκB population will not be quickly phosphorylated and degraded. The best-characterized negative regulators of IKK are the NF-κB-induced deubiquitination enzymes CYLD and A20 (Sun, 2008). Each protein can deubiquitinate substrates upstream of TAB2 and NEMO, including TRAF6, TRAF2, and RIP1. Underscoring the key physiological functions of these deubiquitination enzymes, dysfunction of each protein is associated with disease. CYLD-deficient mice are highly susceptible to

chemically-induced tumors of the skin and colon (Massoumi et al., 2006; Zhang et al., 2006), and mutations in the *Cyld* gene in humans cause familial cylindromatosis—a disorder characterized by tumors of the skin appendages (Bignell et al., 2000). A20-deficient mice spontaneously develop autoimmune disease at an early age, leading to destruction of multiple tissues and premature death (Lee et al., 2000). A20 dysfunction in humans is also associated with autoimmune diseases including systemic lupus erythematosis, and A20 mutations were recently identified in patients with B-cell lymphoma (Compagno et al., 2009; Kato et al., 2009; Schmitz et al., 2009; Verstrepen et al.). The reason for the discrepancy in illnesses caused by dysfunction of CYLD vs. A20 is unknown. Nevertheless, each protein clearly inhibits the NF-κB-regulatory pathways, and it is widely believed that deubiquitination by these two proteins plays an essential role in negative regulation of IKK.

However, with regard to A20, certain data are difficult to reconcile with the proposal that deubiquitination is its primary means of negatively regulating IKK. A detailed summary of the background information on A20 follows in p…., but, briefly, there is evidence suggesting that A20's ability to inhibit NF-κB may not require A20's deubiquitination domain. In addition, it is known that most cells constitutively express a population of A20, suggesting that A20 might exert a negative-regulatory effect prior to its transcriptional induction by NF-κB.

More generally, a clear understanding of the biochemical basis of IKK downregulation, in terms of the proteins involved and their mechanism(s) of action, is lacking. The role of NF-κB-dependent transcription, or for that matter transcription in general, for downregulation of IKK is also not clearly established. Because of the lab's longstanding interest in the mechanisms that activate IKK, and the important gaps in the current understanding of its negative regulation, I undertook projects aimed at gaining insights into the biochemical basis of negative regulation

of IKK. A more detailed background and rationale for each project is discussed within the individual chapters.

Chapter 1

Preliminary results suggesting a non-transcriptional basis for negative regulation of IKK in the IL-1β signaling pathway

Although transcriptional upregulation of inhibitory proteins, such as A20, does occur in response to NF-κB activation (Hayden and Ghosh, 2008), the importance of this transcriptional upregulation, particularly during the initial stages of response to ligand (e.g., first hour), is unknown. To see whether new protein synthesis is required for IKK downregulation, HeLa cells were stimulated with IL-1β in the presence or absence of the protein translation inhibitor cycloheximide, and IKK activity was measured by immunoprecipitating NEMO, then incubating the immunoprecipitate with recombinant GST-IκBα N-terminus and γ-^{32}P-ATP. Remarkably, cycloheximide did not affect the kinetics and magnitude of IKK activity, including the reduction in activity observed after 15 min (Figure 1.1). As a control to make sure that cycloheximide effectively impaired new protein synthesis, IκBα immunoblot was performed on the cell lysate. In contrast to cells without cycloheximide, in which IκBα begins to re-accumulate at 30 and 45 min after IL-1β stimulation, this re-accumulation was not detected in cycloheximide-treated cells. Thus, IKK downregulation occurred without new protein synthesis.

Additional evidence for a non-transcriptional basis for IKK downregulation came from experiments examining desensitization of the IL-1R/TLR4 signaling pathway. HeLa cells which had been previously stimulated with IL-1β for 2 hr were unable to re-activate IKK in response to a second treatment with IL-1β (Figure 1.2, lanes 5-8). If this desensitization is caused by transcriptional upregulation of proteins that non-specifically inhibit IKK, then cells would be predicted to lose responsiveness to other ligands such as TNFα. However, following IL-1β stimulation for 2 hr, cells were able to activate IKK in response to TNFα (Figure 1.2, lanes 9-12). Thus, desensitization appears to be specific to the pathway that was originally activated. The simplest hypothesis to explain these results is that the IL-1β receptor is downregulated following receptor stimulation. I addressed this issue using stable cell lines, previously

Figure 1.1

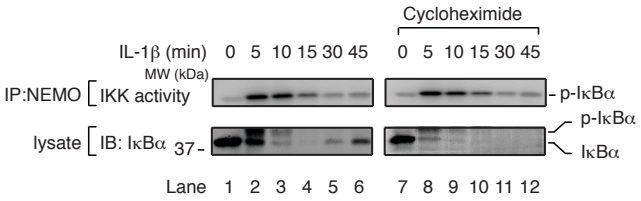

Figure 1.1. IKK downregulation in the IL-1β pathway occurs without new protein synthesis.
HeLa cells were untreated (left) or treated for 30 min with cycloheximide. Cells were further treated with IL-1β for the indicated timepoints. Lysates were used for immunoblots with the indicated antibody or for immunoprecipitation with a NEMO antibody. Immunoprecipitate was used for measurement of IKK activity as described in Experimental Procedures.

Figure 1.2

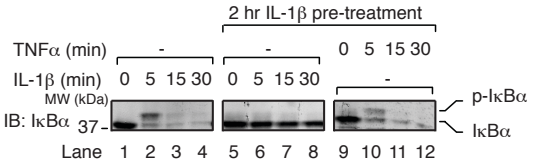

Figure 1.2. Desensitization of IKK signaling is pathway specific.
HeLa cells were untreated (left) or treated for 2 hr with IL-1β. Media was removed and replaced with fresh media. 5 min later, cells were further treated with IL-1β or TNFα for the indicated timepoints. Lysates were immunobloted with antibody against IκBα.

established by the lab, expressing a chimeric protein containing the N-terminal region of TRAF6 fused to the B subunit of bacterial DNA gyrase (gyrB). This protein (T6RZC for TRAF6 RING-Zinc Finger-Coiled Coil), can be activated by adding the small molecule coumermycin, which induces dimerization of the gyrase B domain (Farrar et al., 1996; Wang et al., 2001) (Figure 1.3A, B). Thus, in RAW264.7 cells expressing T6RZC, endogenous TRAF6-dependent IKK activation can be induced extracellularly (with LPS), while T6RZC-dependent IKK activation can be induced intracellularly, bypassing the receptor and upstream signaling machinery. This allowed me to ask whether desensitization of coumermycin-T6RZC signaling would also prevent IKK activation by the endogenous signaling pathway. Strikingly, I found that, following coumermycin stimulation for 2 hr, RAW-T6RZC cells could no longer support coumermycin-induced IKK activation (Figure 1.3C, lanes 13-16). However, coumermycin-desensitized cells were able to support LPS-induced IKK activation (Figure 1.3C, lanes 9-12). Thus, the endogenous TRAF6-dependent signaling pathway had not been desensitized, despite previous TRAF6-dependent activation of IKK with coumermycin. These results suggest that desensitization is "localized" to proteins that have already been activated in the first round of ligand detection. In other words, T6RZC itself appeared to be desensitized following its activation with coumermycin, but the effect was not general to the IL-1R/TLR4 pathway.

Attempts to identify the mechanism(s) by which TRAF6 and/or T6RZC becomes desensitized ultimately led nowhere. I did find, using immunofluorescence, that T6RZC forms large punctate structures following coumermycin treatment (Figure 1.4A). These structures co-localize with similar structures formed by NEMO in these cells, and the kinetics of the formation of these structures correlates with those of IKK activation. However, the relevance of the structures to IKK regulation and/or T6RZC desensitization is unclear. In addition, no such

Figure 1.3

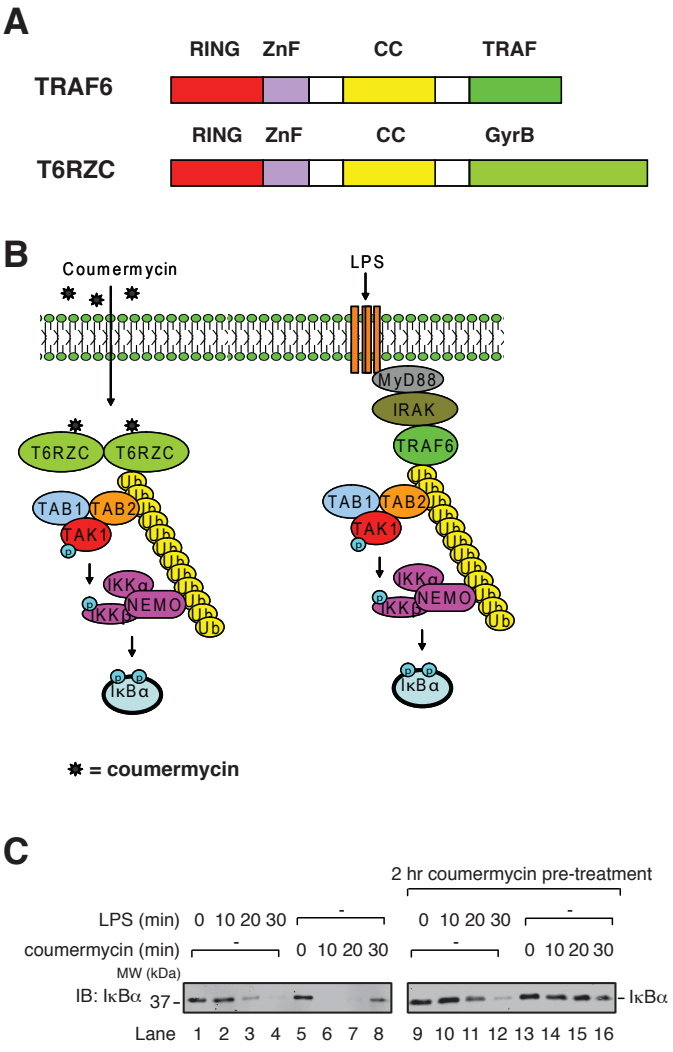

Figure 1.3. Desensitization of IKK signaling is specific to proteins which have been previously activated.
(A) Domain architecture of T6RZC protein. ZnF: zinc finger. CC: coiled coil. GyrB: B subunit of bacterial DNA gyrase. (B) Schematic illustrating the ability of RAW264.7 cells expressing T6RZC to support IKK activation by two TRAF6-dependent pathways. The endogenous pathway can be activated by adding LPS, while an alternative pathway can be activated by adding the small molecule coumermycin, which activates T6RZC. (C) RAW-T6RZC cells were untreated or treated for 2 hr with coumermycin (1 μM). Media was removed and replaced with fresh media. 5 min later, cells were treated with coumermycin or LPS as indicated. Cell lysates were immunoblotted for IκBα.

structures were observed when endogenous TRAF6 or NEMO were immunostained following stimulation of the parental HeLa cells with IL-1β (Figure 1.4B), suggesting that the T6RZC structures, and the resulting NEMO structures in this cell line, may be artifactual.

In any case, though this line of experiments did not lead directly to specific mechanistic insights, its impact on my understanding of IKK downregulation, and the subsequent projects that were undertaken, cannot be overstated. These results, taken together, suggest two foundational hypotheses that have shaped my subsequent work: (1) that non-transcriptional mechanisms suffice to downregulate IKK in the initial stages after ligand detection, and that (2) desensitization of IKK signaling appears to be limited to the specific components that were activated by a ligand (for example, coumermycin or LPS), rather than general to all IKK-regulatory pathways. In other words, desensitization is "localized."

TRAF6 seemed like a sensible candidate as a "target" for desensitization. If TRAF6 was subjected to a desensitization mechanism specific to the TRAF6 population that had been activated, this could explain how another pathway dependent on TRAF6 (for example, T6RZC vs. endogenous TRAF6 in the IL-1R/TLR4 pathway), would remain capable of activating IKK. Thus, I looked for proteins that had been reported to interact with TRAF6 and are known to downregulate IKK. TAX1BP1 and A20 had been reported to fit these two criteria, and the mechanism(s) by which they downregulate IKK became the focus of my project.

Figure 1.4

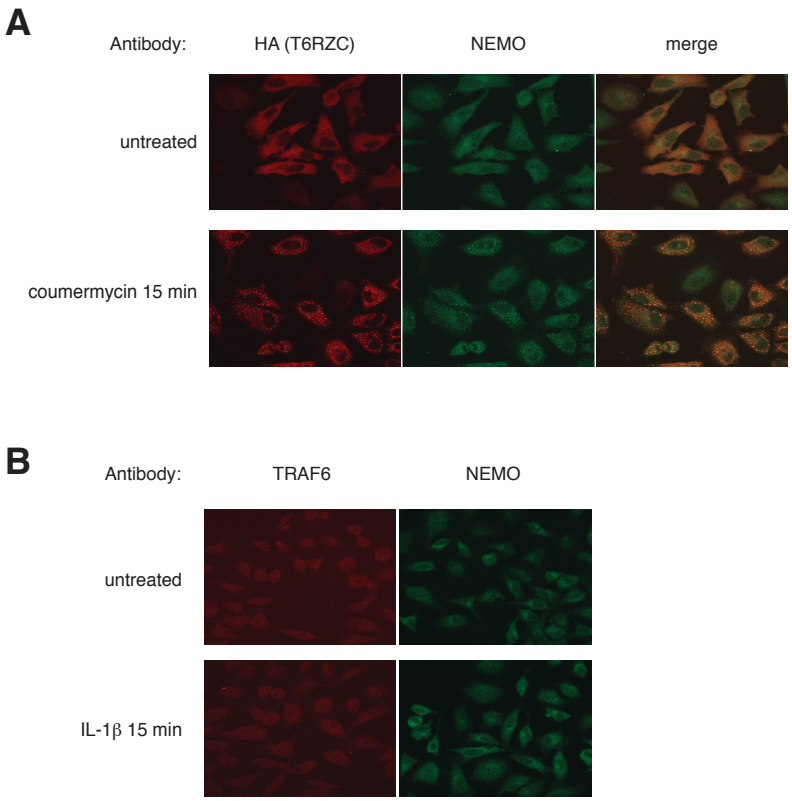

Figure 1.4. T6RZC forms punctate structures upon activation.
HeLa cells stably expressing HA-tagged T6RZC were treated with coumermycin (1 μM) as indicated. Cells were then fixed and stained, using an antibody against HA or NEMO. Images were taken using a confocal microscope. (B) Parental HeLa cells were treated with IL-1β as indicated. Cells were then fixed and stained, using an antibody against TRAF6 or NEMO. Images were taken using a confocal microscope.

Chapter 2

Mechanisms governing IKK inhibition by TAX1BP1

Introduction

A possible role for TAX1BP1 (TAX1-binding protein, also known as T6BP or TRAF6-binding protein) in downregulation of IKK was originally revealed by examining its interactions with other IKK-regulatory proteins. TAX1BP1 interacted with the NF-κB-inhibitory protein A20 in a yeast two-hybrid screen and when overexpressed in mammalian cells (De Valck et al., 1999). In addition, following IL-1β stimulation, TAX1BP1 co-immunoprecipitated with TRAF6 (Ling and Goeddel, 2000). TAX1BP1 was also found to interact with the human T-cell leukemia virus (HTLV-1) oncoprotein TAX, a well-documented activator of IKK (Jin et al., 1997). Yet little was known about the function of TAX1BP1 until mice deficient in TAX1BP1 were generated (Iha et al., 2008; Shembade et al., 2007). These mice developed autoimmune attack of the cardiac valves and were hypersusceptible to challenge with TNFα and IL-1β. Moreover, cells lacking TAX1BP1 had enhanced IKK activation in response to these ligands. TAX1BP1 was shown to interact with A20 and promote its recruitment to RIP1 and TRAF6. Moreover, TAX1BP1's C-terminal ZnF motifs were found to bind to K63-linked polyubiquitin chains, and this binding was required for NF-κB downregulation. Based on these results it was proposed that TAX1BP1 facilitates delivery of A20 to ubiquitinated RIP1 and TRAF6, facilitating their deubiquitination and thus downregulation of the signaling pathway.

Although these reports present convincing evidence that TAX1BP1 is an important suppressor of IKK signaling, evidence for the proposed mechanism of action left room for doubt. For example, the role of covalent modification of TRAF6 with polyubiquitin chains in IKK regulation is unclear, and our lab has shown the unanchored polyubiquitin chains can activate TAK1 and IKK (Xia et al., 2009). Therefore antagonizing ubiquitination of TRAF6 might not necessarily affect IKK activity. In any case, the more fundamental issue is that the majority of

conclusions regarding the mechanism of IKK inhibition by TAX1BP1 were gleaned from experiments where TAX1BP1 was overexpressed, followed by a series of immunoprecipitation/Western blotting experiments to examine its interacting partners. The results from these experiments are consistent with the conclusions that the authors' reached, but do not rule out alternative explanations. I thought that our lab's cell-free biochemical systems might allow clarification of the mechanism(s) by which TAX1BP1 inhibits IKK.

In vitro inhibition of TAK1 and IKK

To gain insights into the mechanism(s) by which TAX1BP1 inhibits IKK, I utilized a cell-free assay that partially recapitulates the IL-1β signaling pathway (Deng et al., 2000). In this assay, recombinant TRAF6 protein is added to cytosolic extract (S100), along with ATP. This leads to activation of the endogenous pool of TAK1 and IKK, resulting in TAK1 phosphorylation on Thr-187 and IκBα phosphorylation that is clearly detectable because of a gel shift on SDS-PAGE. GST-TAX1BP1 was expressed in SF9 cells using baculovirus, then purified by glutathione sepharose. The GST tag was cleaved with TEV protease, and TAX1BP1 was further purified by anion exchange on a HiTrap Q column. This TAX1BP1 was able to impair TAK1 and IKK activation in S100 downstream of TRAF6, as evidenced by the failure of TRAF6 to induce TAK1 Thr-187 phosphorylation or IκBα phosphorylation (Figure 2.1A). To see if IKK inhibition in vitro by TAX1BP1 depends on A20, the assay was performed in S100 from $A20^{-/-}$ MEFs or the corresponding $A20^{+/+}$ MEFs. TAX1BP1 impaired IKK activation as potently in S100 lacking A20 as it did in S100 with A20 (Figure 2.1B), suggesting that, in this experimental system, TAX1BP1 impairs IKK activation independently of A20.

To identify domains of TAX1BP1 required for this inhibition, deletion mutants of TAX1BP1 lacking the first two coiled coils (444-789), the ZnF motifs (444-727), or all three coiled coils (602-789) were purified from E.Coli (Figure 2.1C-D). Deletion of the ZnF motifs, but not deletion of the coiled coils, abolished the ability of TAX1BP1 to inhibit IKK (Figure 2.1E). The mutant lacking all three coiled coils (602-789) was slightly less potent than the mutant containing the 3rd coiled coil (444-789) and the WT protein (1-789), suggesting a minor role for the 3rd coiled coil. The ZnF region of TAX1BP1 can bind to K63-linked polyubiquitin chains (Iha 2008), but it is unknown whether other regions of TAX1BP1 contribute to polyubiquitin binding. To assay polyubiquitin binding, GST-TAX1BP1 and the deletion mutants were mixed with K63-linked tetraubiquitin, then GST pull-down was performed. Full-length TAX1BP1 and the mutants containing the ZnF region bound to similar amounts of K63 tetraubiquitin, while the mutant lacking the ZnF region (444-789) did not detectably bind (Figure 2.1F). Thus, the ZnF region is necessary and sufficient for binding to K63-linked polyubiquitin chains.

To see whether TAX1BP1 can directly impair TAK1 activation, I utilized an assay in which polyubiquitin-dependent TAK1 activation is reconstituted with purified proteins (Xia 2009). In this assay, K63-linked polyubiquitin chains are synthesized by recombinant E1, UBC13/UEV1A, and TRAF6 (Figure 2.2A-C). The E1 and E2 enzymes are then inactivated using N-ethyl-maleamide (NEM), which alkylates Cys residues (ubiquitin is unaffected by NEM because it has no Cys residues). Following buffer exchange to remove NEM, this mixture has the ability to activate purified TAK1 complex, which can be detected by immunoblotting for TAK1 Thr-187 phosphorylation, or, by phosphorylation of a kinase-dead mutant of the MAP2K MKK6 (K82A) (Figure 2.2D). TAX1BP1 WT and mutants containing the ZnF region were able

Figure 2.1

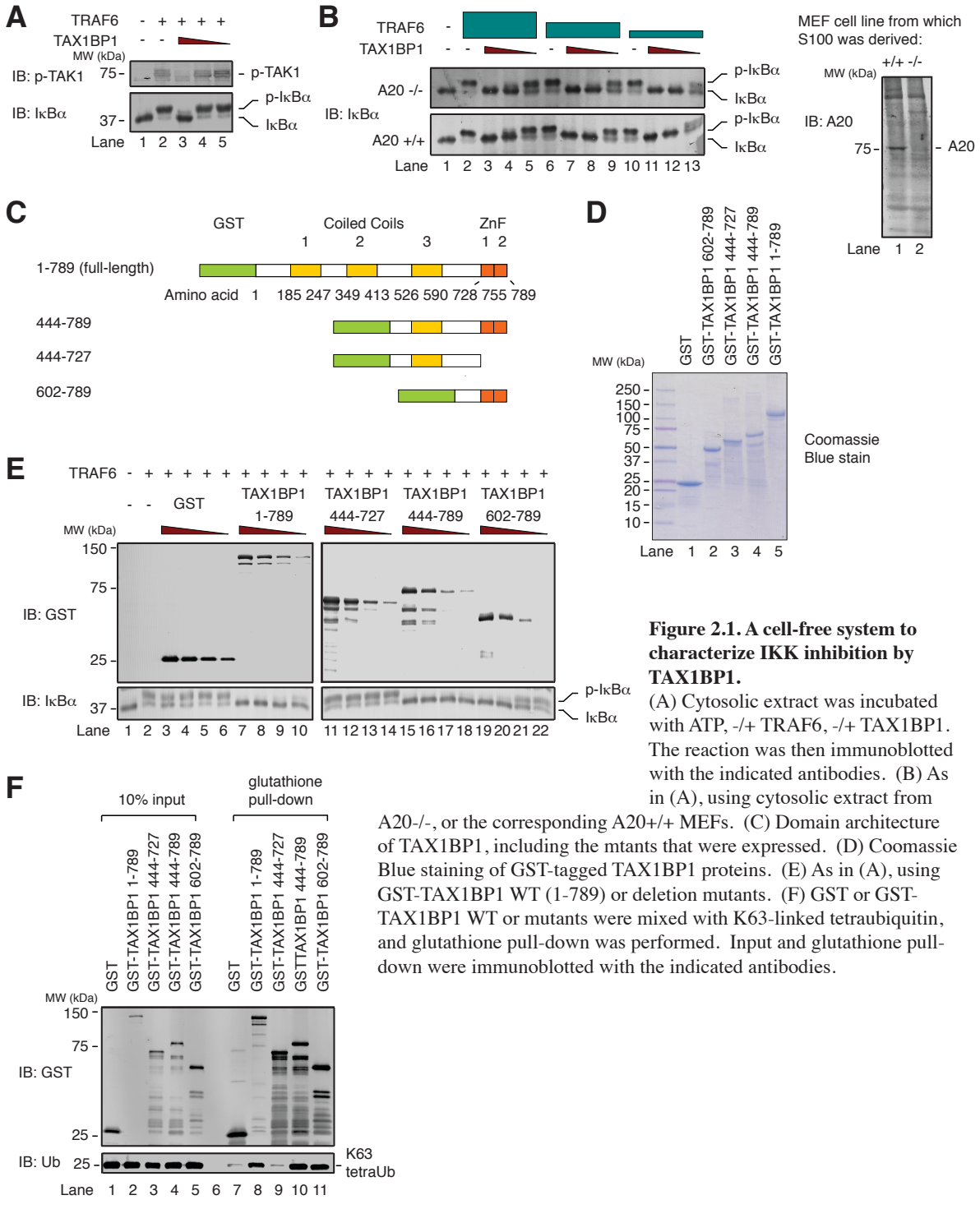

Figure 2.1. A cell-free system to characterize IKK inhibition by TAX1BP1.
(A) Cytosolic extract was incubated with ATP, -/+ TRAF6, -/+ TAX1BP1. The reaction was then immunoblotted with the indicated antibodies. (B) As in (A), using cytosolic extract from A20-/-, or the corresponding A20+/+ MEFs. (C) Domain architecture of TAX1BP1, including the mtants that were expressed. (D) Coomassie Blue staining of GST-tagged TAX1BP1 proteins. (E) As in (A), using GST-TAX1BP1 WT (1-789) or deletion mutants. (F) GST or GST-TAX1BP1 WT or mutants were mixed with K63-linked tetraubiquitin, and glutathione pull-down was performed. Input and glutathione pull-down were immunoblotted with the indicated antibodies.

Figure 2.2

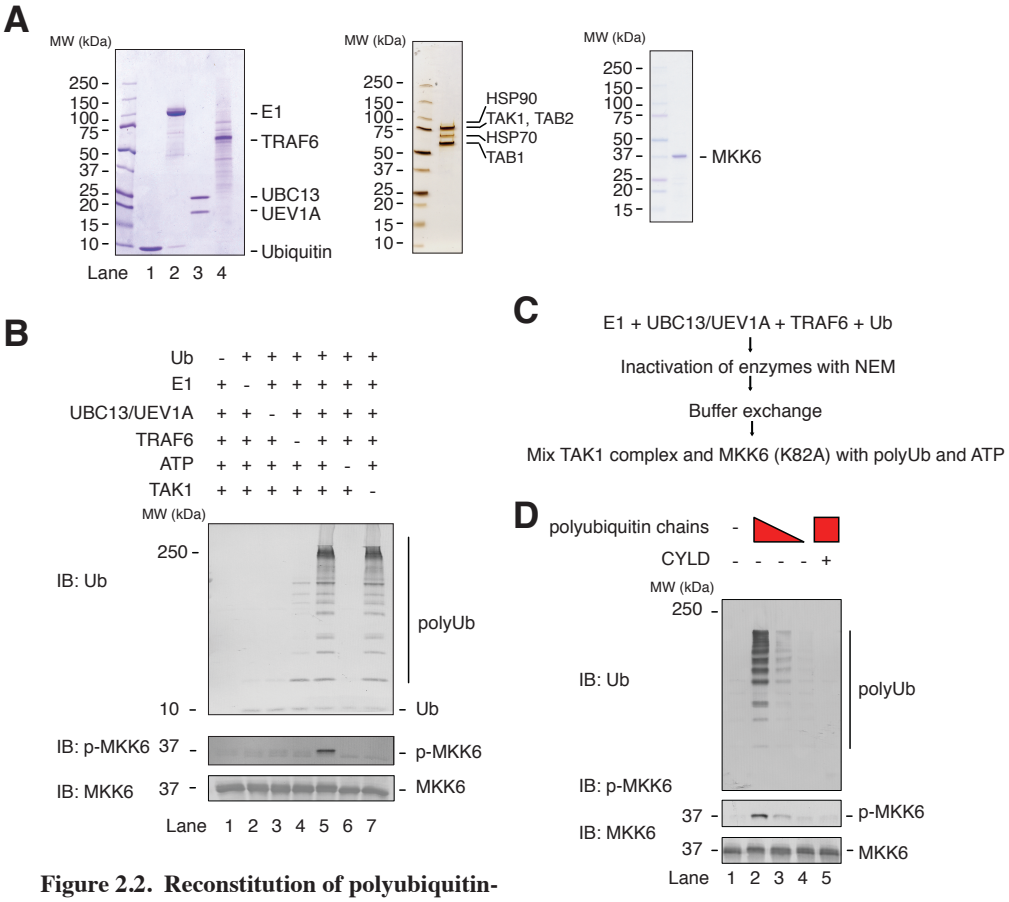

Figure 2.2. Reconstitution of polyubiquitin-dependent TAK1 activation using purified proteins.
(A) (Left) Coomassie Blue staining of ubiquitin and ubiquitination enzymes. (Middle) Silver staining of affinity-purified TAK1 complex. Proteins were identified by mass spectrometry. (Right) Coomassie Blue staining of His6-MKK6 (K82A). (B) Ubiquitination components, TAK1 complex, and ATP were mixed in various combinations with MKK6 (K82A). Only when each component is present (lane 5) is MKK6 phosphorylation observed. (C) Schematic of strategy to uncouple polyubiquitin chain synthesis from activation of TAK1 kinase. (D) TAK1 complex and MKK6 (K82A) were incubated with ATP, -/+ pre-synthesized polyubiquitin chains, -/+ the K63-deubiquitination enzyme CYLD. Reaction was immunoblotted with the indicated antibodies.

to impair TAK1 activation, whereas a mutant lacking the ZnF region was not (Figure 2.3A). Thus, TAX1BP1 can directly impair TAK1 activation in a manner dependent on its ubiquitin binding domain. The simplest explanation for this result is that TAX1BP1 competes with TAB2 for binding to K63-linked polyubiquitin chains. Indeed, in the presence of GST-TAX1BP1, but not GST alone, pull-down of K63-linked tetraubiquitin by TAB2 was impaired (Figure 2.3B).

These results strongly suggest that TAX1BP1 harbors the ability to directly impair TAK1 activation by competitively inhibiting the binding of TAB2 to polyubiquitin chains. Although not tested, it is likely that TAX1BP1 could also impair binding of NEMO to polyubiquitin chains. Although these results highlight the key role of polyubiquitin binding for activation of TAK1 and IKK, as well as the ability of the reconstitution assay system to detect direct inhibition of these kinases, caution must be taken in extrapolating the results to the TNFα and IL-1β signaling pathways in vivo. The fact that a polyubiquitin binding protein can impair TAK1 and IKK activation in these assays is predictable, and by itself, largely uninformative. In fact, any polyubiquitin binding protein is expected to cause inhibition in these assays if added in sufficient quantity, and I have found that S5A, a proteasomal subunit with a ubiquitin binding domain, is also sufficient to impair TAK1 and IKK activation (data not shown). Currently there is no evidence that TAX1BP1 competes with TAB2 or NEMO for polyubiquitin binding in cells, or can facilitate TAK1 and IKK inhibition in the absence of A20. Because of developments in other aspects of my thesis work (see below), experiments to test this idea were not undertaken.

Regulated interaction between TAX1BP1 and A20

TAX1BP1-A20 binding was postulated as a means of delivering A20 to ubiquitinated substrates (Iha et al., 2008; Shembade et al., 2007). However, whether the TAX1BP1-A20

Figure 2.3

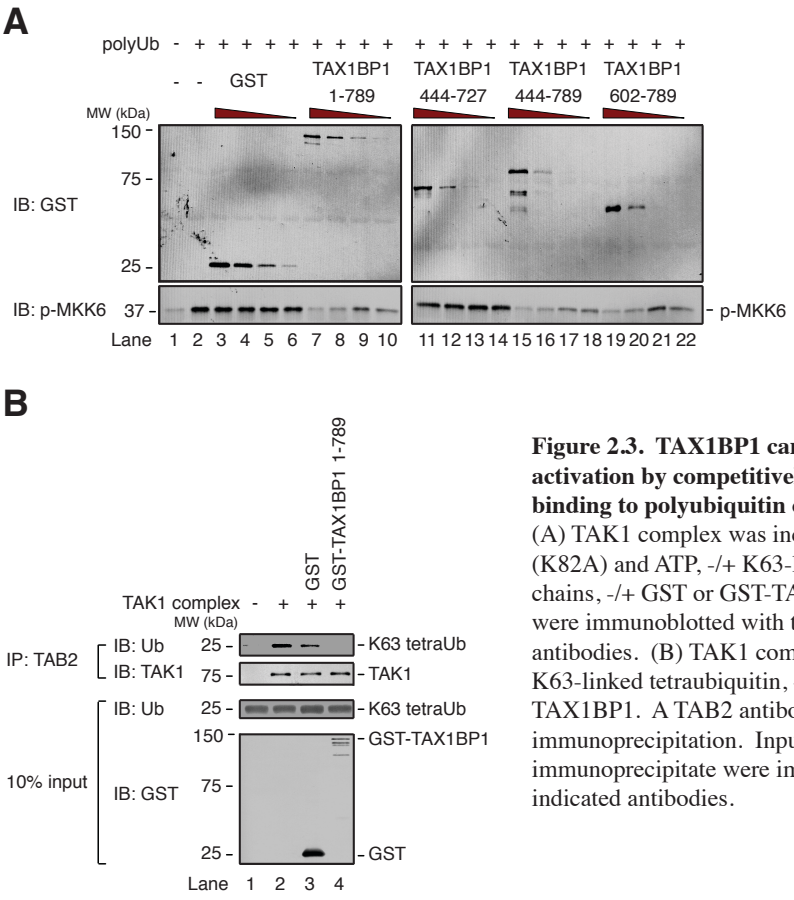

Figure 2.3. TAX1BP1 can directly impair TAK1 activation by competitively inhibiting TAB2 binding to polyubiquitin chains..
(A) TAK1 complex was incubated with MKK6 (K82A) and ATP, -/+ K63-linked polyubiquitin chains, -/+ GST or GST-TAX1BP1. Reactions were immunoblotted with the indicated antibodies. (B) TAK1 complex was incubated -/+ K63-linked tetraubiquitin, -/+ GST or GST-TAX1BP1. A TAB2 antibody was used for immunoprecipitation. Input and immunoprecipitate were immunoblotted with the indicated antibodies.

interaction itself is regulated has not been addressed. In fact, the interaction has only been observed when one or both proteins were overexpressed. However, IL-1β-induced interaction between endogenous TAX1BP1 and TRAF6 had been previously observed (Ling and Goeddel, 2000). To assess whether TAX1BP1's interaction with A20 might also be regulated, I attempted to immunoprecipitte TAX1BP1 and immunoblot for A20. Unfortunately I was unable to immunoprecipitate a detectable amount of TAX1BP1 using a commercial anti-TAX1BP1 antibody (data not shown).

I therefore prepared a recombinant fragment of TAX1BP1 (residues 13-128) for inoculation of rabbits for a new antibody. This fragment of TAX1BP1 was cloned in the GATEWAY expression system (Invitrogen) into a vector for E. Coli expression with an N-terminal GST tag followed by a TEV protease cleavage site. Following purification of GST-TAX1BP1 (13-128) with glutathione sepharose, and elution with reduced glutathione, the eluate was incubated overnight with TEV protease. To separate TAX1BP1 (13-128) from GST and TEV protease, the sample was run on a HiTrap Q column. 2 mg of purified TAX1BP1 (13-128) protein was sent to Rockland Immunochemicals, Inc., for immunization of two rabbits. The test serum was able to detect ~1 ng of TAX1BP1 (13-128) (data not shown). Anti-TAX1BP1 antibody was purified from the test serum using an antigen column composed of TAX1BP1 (13-128) coupled to NHS sepharose.

Using this purified antibody, I found that TAX1BP1 co-immunoprecipitated A20 in an IL-1β-dependent manner (Figure 2.4). This observation was of great interest because it immediately suggested a possible mechanism of negative feedback of the signaling pathway. Given the premise that TAX1BP1-A20 interaction is important for negative regulation of the

Figure 2.4

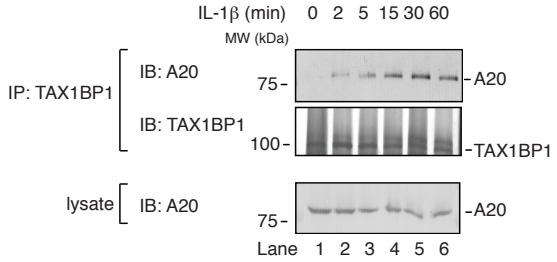

Figure 2.4. Interaction between endogenous TAX1BP1 and A20 is regulated.
HeLa cells were stimulated with IL-1β for the indicated timepoints. Lysates were used for immunoprecipitation with an antibody against TAX1BP1. Lysate and immunoprecipitate were immunoblotted with the indicated antibodies.

pathway, I hypothesized that some "activating" signal was inducing the TAX1BP1-A20 interaction, leading to suppression of the pathway upstream of this signal.

The most obvious candidate for a signal to induce TAX1BP1-A20 interaction was phosphorylation by IKK. Since IKK is the most downstream component of the pathway leading to IκBα phosphorylation, it seems well-positioned to promote a negative feedback loop that would ultimately result in its inactivation. In addition, A20 was previously identified as an IKK substrate (Hutti et al., 2007). This phosphorylation, on A20 Ser 381, was proposed to promote negative feedback through an unidentified mechanism. I also found that IKK can phosphorylate TAX1BP1 in vitro in a stimulus-dependent manner (Figure 2.5). I therefore hypothesized that phosphorylation of A20 and/or TAX1BP1 by IKK is the signal to induce TAX1BP1-A20 interaction, and that IKK phosphorylation therefore promoted negative feedback of the pathway.

In support of this hypothesis, A20 did not co-immunoprecipitate with TAX1BP1 following TNFα stimulation of NEMO$^{-/-}$ Jurkat cells (Figure 2.6A). This result suggested either that NEMO plays a direct role in TAX1BP1-A20 interaction, or that IKK activation is required for TAX1BP1-A20 interaction. To distinguish between these possibilities, HEK293 cells were treated with the small molecule inhibitor of IKK, TPCA-1. To my great surprise, TPCA-1 dramatically enhanced TAX1BP1-A20 interaction (Figure 2.6B). This enhancement appeared to be specific to TAX1BP1 and A20, because co-immunoprecipitation of RIP1 was minimally affected by TPCA-1. This result suggests that, contrary to my hypothesis, IKK actually impairs TAX1BP1-A20 interaction. In addition, the result implies that an alternative factor is required for TAX1BP1-A20 interaction to occur.

To facilitate biochemical manipulation of the signaling pathway and to rule out transcriptional regulation, I attempted to recapitulate the regulated TAX1BP1-A20 interaction in

Figure 2.5

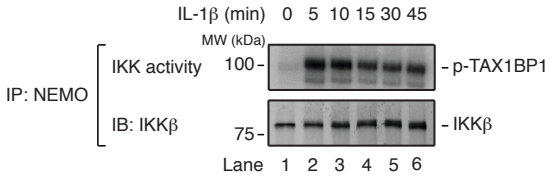

Figure 2.5. IKK can phosphorylate TAX1BP1 in vitro.
HeLa cells were treated with IL-1β for the indicated timepoints, and a NEMO antibody was used for immunoprecipitation. Immunoprecipitate was incubated with recombinant TAX1BP1 and γ-32P-ATP. To ensure equal amounts of IKKβ were present in each sample, IKKβ immunoblot was performed.

Figure 2.6

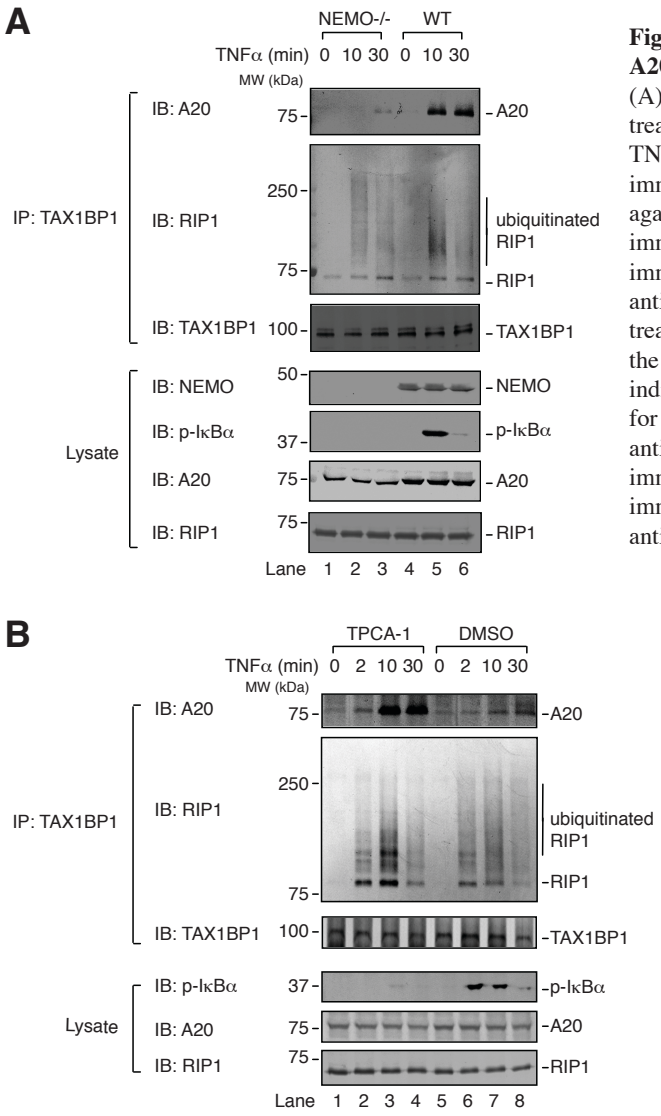

Figure 2.6. Regulation of TAX1BP1-A20 interaction by the IKK complex. (A) NEMO-/- or WT Jurkat cells were treated for the indicated timepoints with TNFα. Lysates were used for immunoprecipitation with an antibody against TAX1BP1. Lysates and immunoprecipitates were immunoblotted with the indicated antibodies. (B) HEK293 cells were treated with TPCA-1 or DMSO. Then, the cells were treated with TNFα for the indicated timepoints. Lysates were used for immunoprecipitation with an antibodyagainst TAX1BP1. Lysates and immunoprecipitates were immunoblotted with the indicated antibodies.

cytosolic extract. Indeed, in the presence TRAF6 and TPCA-1, but not either by itself, GST-TAX1BP1 pulled down endogenous A20 from cytosolic extract (Figure 2.7A). An alternative small molecule inhibitor of IKK, BMS-345541, also promoted TAX1BP1-A20 interaction (Figure 2.7B). Importantly, neither small molecule inhibitor impaired TAK1 phosphorylation, suggesting that the effect on TAX1BP1-A20 interaction was specific to inhibition of IKK. To determine whether NEMO is required for TAX1BP1-A20 interaction in vitro, NEMO was immunodepleted. Remarkably, in NEMO-depleted cytosolic extract, TAX1BP1-A20 interaction was abolished (Figure 2.7C). These results suggest that NEMO plays a role in promoting TAX1BP1-A20 interaction independent of its role in activation of IKK.

The fact that TRAF6 is also required for TAX1BP1-A20 interaction in vitro suggests either that TRAF6, or the polyubiquitin chains synthesized by TRAF6, act as a scaffold upon which TAX1BP1 and A20 assemble into a complex. To distinguish between these possibilities, TRAF6 was uncoupled from the accumulation of polyubiquitin chains using two independent methods: (1) addition of excess deubiquitination enzyme—the OTU domain from Crimean Congo Hemorrhagic Fever Virus (CCHFV) L1 protein, or, (2) depletion of UBC13. In either case, TAX1BP-A20 interaction was abolished (Figure 2.8A). Importantly, the TAX1BP1-A20 interaction was rescued in the UBC13-depleted cytosolic extract by adding back recombinant His_6-UBC13 (lanes 10-12). This result strongly suggests that K63-linked polyubiquitin chains induce TAX1BP1-A20 interaction. In support of this hypothesis, TAX1BP1 ΔZnF (444-727) did not interact with A20 under these conditions, whereas TAX1BP1 (444-789) interacted as well as TAX1BP1 WT (Figure 2.8B). Interestingly, TAX1BP1 (602-789), which lacks all three coiled coil domains, pulled down less A20 than TAX1BP1 WT, suggesting that, in addition to its ubiquitin binding domain, another region of TAX1BP1 is important for interaction with A20.

Figure 2.7

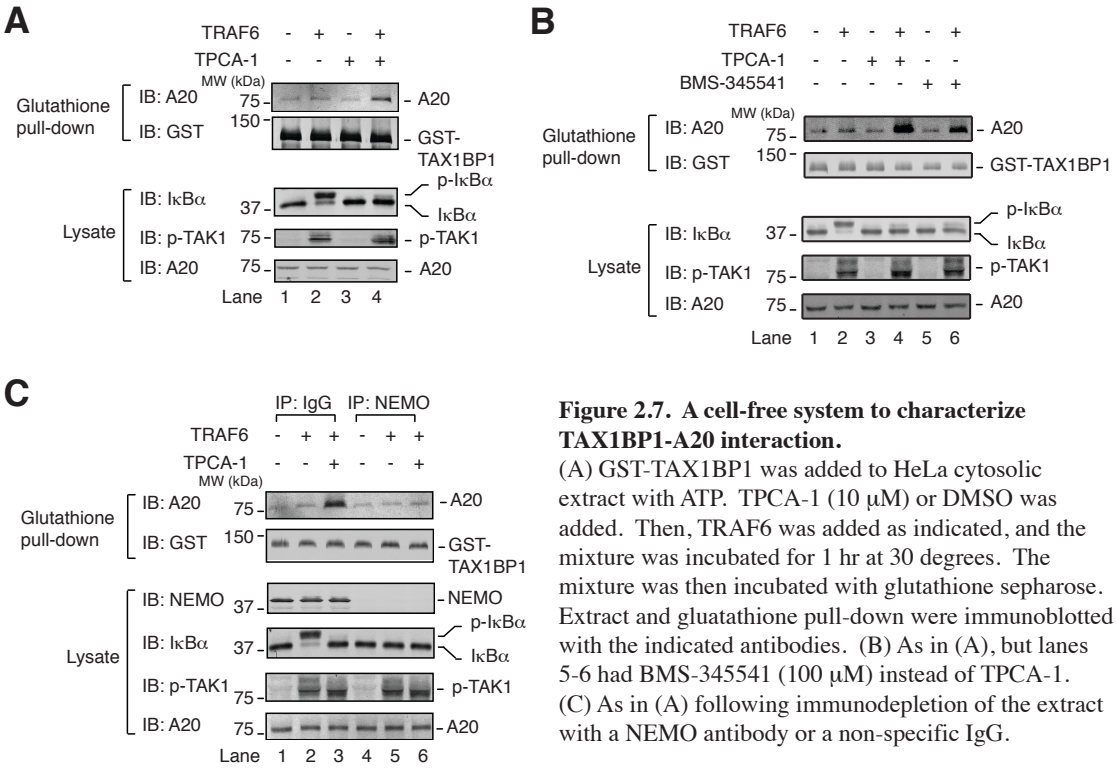

Figure 2.7. A cell-free system to characterize TAX1BP1-A20 interaction.
(A) GST-TAX1BP1 was added to HeLa cytosolic extract with ATP. TPCA-1 (10 μM) or DMSO was added. Then, TRAF6 was added as indicated, and the mixture was incubated for 1 hr at 30 degrees. The mixture was then incubated with glutathione sepharose. Extract and gluatathione pull-down were immunoblotted with the indicated antibodies. (B) As in (A), but lanes 5-6 had BMS-345541 (100 μM) instead of TPCA-1. (C) As in (A) following immunodepletion of the extract with a NEMO antibody or a non-specific IgG.

Figure 2.8

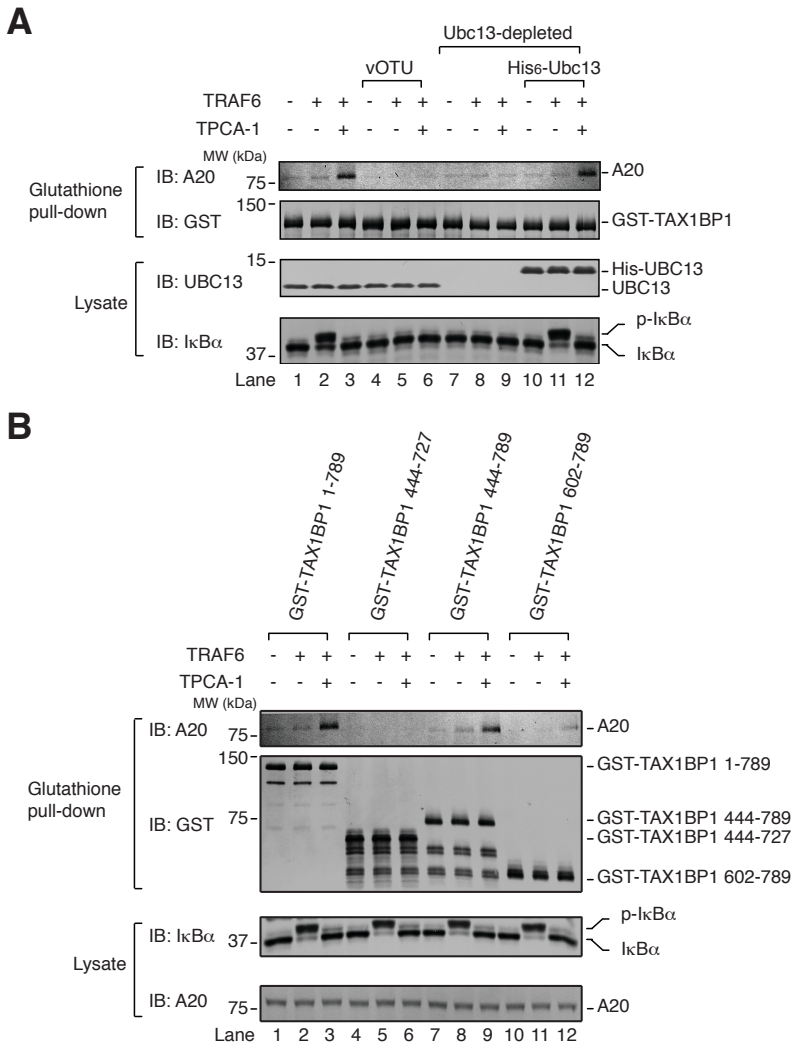

Figure 2.8. Polyubiquitin chains mediate TAX1BP1-A20 interaction in cytosolic extract. (A) As in Figure 2.6(A), following depletion of UBC13 and/or addition of recombinant vOTU or His6-UBC13. (B) As in Figure 2.6(A), except various truncation mutants of TAX1BP1 were used.

Taken together, these results strongly suggest that interaction between TAX1BP1 and A20 is regulated by multiple factors. NEMO and polyubiquitin chains appear to be required for the interaction, while phosphorylation by IKK inhibits it. Characterization of the TAX1BP1-A20 interaction was not pursued further, but these results led to some important ideas that shaped my thinking in subsequent experiments. First, the idea that polyubiquitin chains can promote protein-protein interactions was pivotal in investigating the mechanism by which A20 inhibits IKK (see below). Secondly, the loss of TAX1BP1-A20 interaction in the absence of NEMO suggested the assembly of a multi-protein complex containing NEMO and A20. When I later began looking for a non-catalytic mechanism of IKK inhibition by A20 (discussed below), the idea that NEMO and A20 might be in a complex was highly influential. Whether TAX1BP1-A20 interaction actually requires polyubiquitin chains in vivo remains to be tested. Moreover, the requirement of NEMO for TAX1BP1-A20 interaction requires further testing, including rescue experiments in vitro and/or in the $NEMO^{-/-}$ cells. The ability of IKK to impair TAX1BP1-A20 interaction also remains unexplained (discussed in more detail in the next section). These thoughts were not pursued further because of a shift in emphasis to the elucidation of a non-catalytic mechanism of IKK inhibition by A20.

Chapter 3

Direct, non-catalytic mechanism of IKK inhibition by A20

Introduction

A20 is a potent suppressor of the NF-κB signaling pathways, and A20 deficiency in mice results in excess NF-κB activity and multiorgan inflammation (Boone et al., 2004; Lee et al., 2000). Recent evidence also implicates dysfunction of A20 as a risk factor for human disease. Polymorphisms in the A20 locus are associated with multiple autoimmune diseases including systemic lupus erythematosis, and A20 was recently identified as a tumor suppressor in B-cell lymphoma (Compagno et al., 2009; Kato et al., 2009; Musone et al., 2008; Schmitz et al., 2009; Vereecke et al., 2009). A20 has an N-terminal ovarian tumor (OTU) domain and seven C-terminal zinc finger (ZnF) motifs. The OTU domain can deubiquitinate RIP1, and the ZnF region can act as an E3 ligase to add K48 polyubiquitin chains to RIP1, promoting its proteasomal degradation (Wertz et al., 2004). A20 also promotes disassembly of ubiquitination complexes in the IL-1R and TNFR pathways, including TRAF6-UBC13; cIAP1/2-UBC13; and cIAP1/2-UBCH5, as well as proteasomal degradation of UBC13 and UBCH5 (Shembade et al., 2010). Importantly, both deubiquitination and disassembly of E2-E3 complexes require A20's catalytic Cys 103 residue within the OTU domain. A20 has also been reported to block recruitment of the adaptor proteins TRADD and RIP1 to the TNFR (He and Ting, 2002), and to promote lysosomal degradation of TRAF2 (Li et al., 2009). Although the relative contributions of deubiquitination, degradation of upstream signaling proteins, and disruption of ubiquitination complexes remain unclear, A20 appears to employ multiple mechanisms that could potentially reduce the amount of polyubiquitin chains available to interact with TAB2 and NEMO.

Yet certain data are difficult to reconcile with the proposed catalytic mechanisms. For example, in vitro, A20's OTU domain readily disassembles K48 polyubiquitin chains, but only weakly disassembles K63 polyubiquitin chains (Komander and Barford, 2008; Lin et al., 2008).

In addition, overexpression of A20 mutants lacking the catalytic Cys 103 residue inhibits NF-κB, suggesting a non-catalytic mechanism (Evans et al., 2004; Song et al., 1996). Perhaps more importantly, the notion that A20 reduces the amount of polyubiquitin chains available to interact with TAB2 and NEMO is untested.

Evidence suggesting a non-catalytic mechanism of IKK inhibition by A20

As a tool to dissect the mechanism of IKK inhibition by A20, I stably overexpressed A20 in HEK293 cells that express IL-1R. In this cell line, TNFα-induced IKK activation was severely impaired compared to the parental cells, as evidenced by the lack of IκBα degradation and the failure of immunoprecipitated IKK complex to phosphorylate IκBα (Figure 3.1A). To test whether IKK inhibition in this cell line was caused by disruption of the TNFR complex, I stimulated cells with GST-TNFα, then pulled down the TNFR complex using glutathione sepharose and immunoblotted for TRADD and RIP1. Strikingly, TRADD and RIP1, including a high molecular weight smear of RIP1 indicative of ubiquitination, were enriched on TNFR in A20-overexpression cells compared to parental cells (Figure 3.1B). Notably, A20 was recruited to this complex. I also immunoprecipitated NEMO from TNFα-treated cells and compared the abundance of ubiquitinated RIP1 that interacted with NEMO in A20-overexpression vs. parental cells. Remarkably, NEMO co-immunoprecipitated more ubiquitinated RIP1 from the A20-overexpression cells (Figure 3.1C). Notably, A20 was also recruited to this complex. Thus, overexpressed A20 was recruited to the NEMO-RIP1 complex and inhibited IKK activation, apparently without deubiquitinating RIP1, causing degradation of RIP1, inhibiting ubiquitination of RIP1, or disrupting the interaction of NEMO with polyubiquitinated RIP1. In support of a

non-catalytic mechanism of IKK inhibition, stable overexpression of A20 C103A also suppressed TNFα-induced IκBα degradation (Figure 3.1D).

Notably, A20 overexpression also impaired TNFα-induced TAK1 activation (Figure 3.2A). This result was slightly ambiguous because, for unknown reasons, TAK1 basal activity was higher in A20-overexpressing cells compared to parental cells (lane 1 vs. lane 5). Nevertheless, following TNFα stimulation, TAK1 activation was weaker when A20 was overexpressed (lanes 2-4 and 6-8). As was the case with NEMO, TAB2 had enhanced interaction with ubiquitinated RIP1 in A20-overexpressing cells, and A20 was recruited to TAB2 in a TNFα-dependent manner (Figure 3.2B).

To dissect the mechanism of IKK inhibition by A20, I wished to test whether purified A20 protein could inhibit IKK activation by TRAF6 in S100. However, A20 was almost completely insoluble when expressed in SF9 cells (data not shown). As an alternative approach, I transfected into HEK293 cells a construct in which A20 contains an N-terminal tandem affinity purification (TAP) tag, consisting of a protein-A fragment and a calmodulin binding peptide (CBP) separated by a TEV protease site, and a C-terminal Flag tag. A20 was purified from this cell line by two-step affinity purification (IgG-Sepharose followed by anti-Flag antibody Sepharose) (Figure 3.3A). This A20 impaired IKK activation by TRAF6 (Figure 3.3B). A20 Cys 103, although required for deubiquitination and disruption of ubiquitination complexes, was dispensable for this activity, because its mutation to Ala (C103A) had no effect on IKK inhibition (lanes 6-8).

This combination of results dramatically changed the emphasis of my project. Whereas before it seemed likely that deubiquitination plays a major role in inhibition of IKK activation, my results suggest that, at least under conditions where A20 is in excess, deubiquitination plays

Figure 3.1

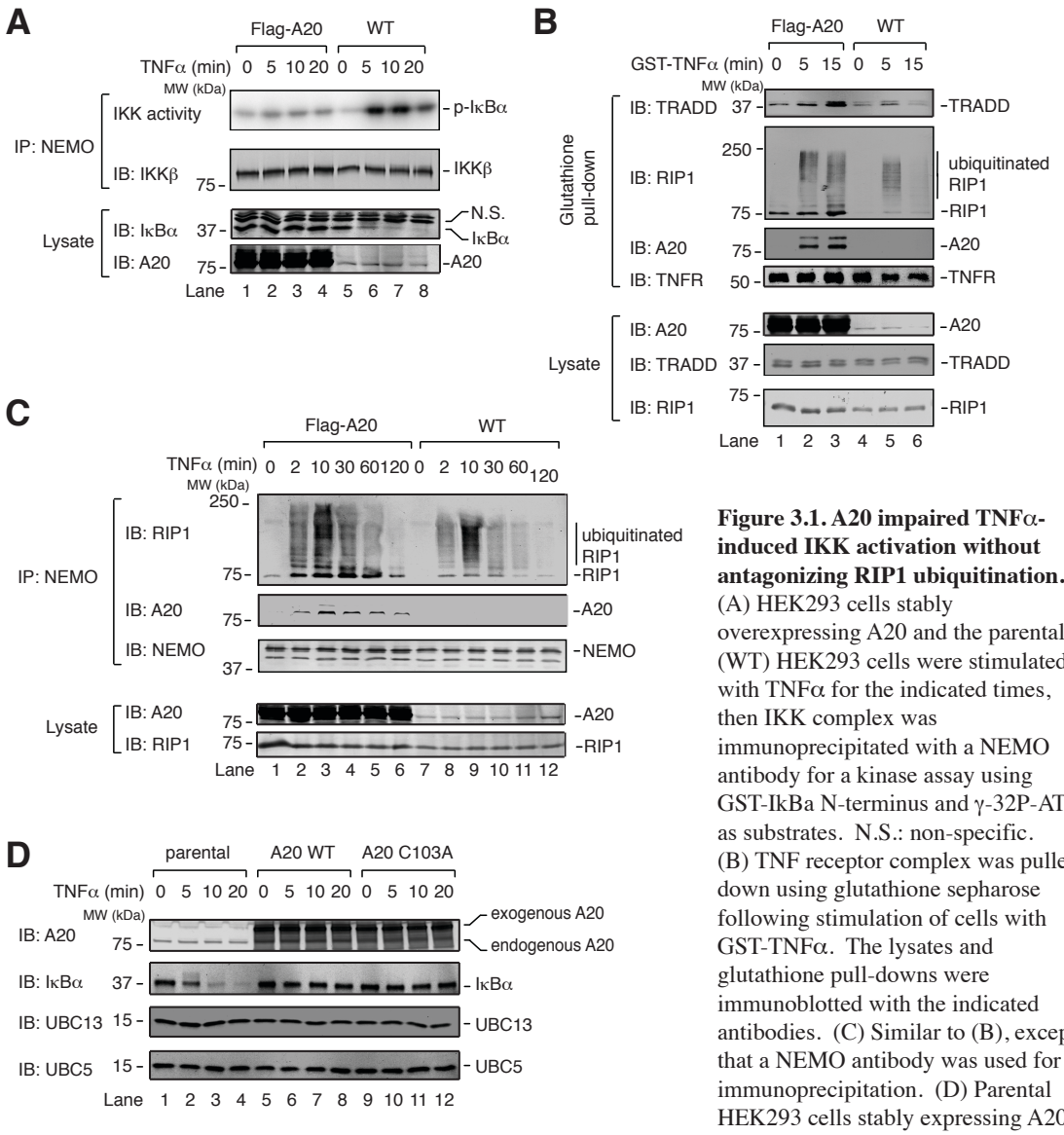

Figure 3.1. A20 impaired TNFα-induced IKK activation without antagonizing RIP1 ubiquitination. (A) HEK293 cells stably overexpressing A20 and the parental (WT) HEK293 cells were stimulated with TNFα for the indicated times, then IKK complex was immunoprecipitated with a NEMO antibody for a kinase assay using GST-IkBa N-terminus and γ-32P-ATP as substrates. N.S.: non-specific. (B) TNF receptor complex was pulled down using glutathione sepharose following stimulation of cells with GST-TNFα. The lysates and glutathione pull-downs were immunoblotted with the indicated antibodies. (C) Similar to (B), except that a NEMO antibody was used for immunoprecipitation. (D) Parental HEK293 cells stably expressing A20 WT or C103A with N-terminal TAP tag and C-terminal Flag tag were treated with TNFα for the indicated times. Cell lysates were used for immunoblotting with the indicated antibodies.

Figure 3.2

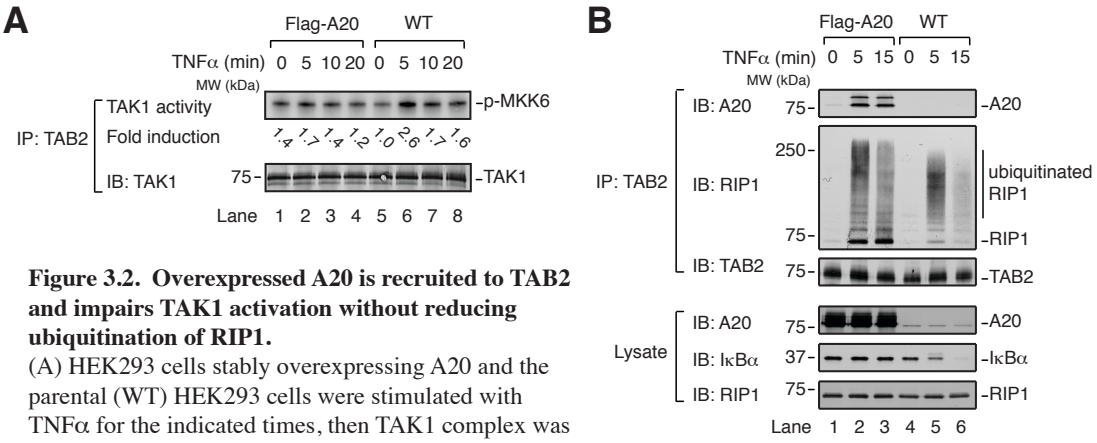

Figure 3.2. Overexpressed A20 is recruited to TAB2 and impairs TAK1 activation without reducing ubiquitination of RIP1.
(A) HEK293 cells stably overexpressing A20 and the parental (WT) HEK293 cells were stimulated with TNFα for the indicated times, then TAK1 complex was immunoprecipitated with a TAB2 antibody for a kinase assay using His6-MKK6 (K82A) and γ-32P-ATP as substrates. (B) HEK293 cells stably overexpressing A20 and the parental (WT) HEK293 cells were stimulated with TNFα for the indicated times, and lysates were used for immunoprecipitation with an antibody against TAB2. Lysates and immunoprecipitates were immunoblotted with the indicated antibodies.

Figure 3.3

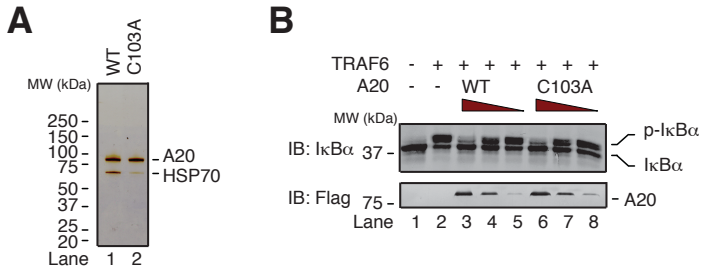

Figure 3.3. A20 Cys103 is dispensable for inhibition of IKK in cytosolic extract.
(A) Silver stain of two-step affinity purified A20. Proteins were idenified by mass spectrometry. HSP70: 70 kDa heat shock protein. (B) Different amounts of purified A20 (WT or C103A) were incubated with HeLa cytosolic extract and ATP, followed by incubation with TRAF6. IKK activation was measured by immunoblotting for IκBα.

little if any role. Therefore, my results challenge the major premise that has dominated thought on A20 for the past few years. Instead of focusing on the mechanisms that facilitate deubiquitination of substrates upstream of A20 (e.g., delivery of A20 to ubiquitinated RIP1 by TAX1BP1), I focused instead on the opportunity to elucidate a fundamentally different mechanism by which A20 impairs IKK activation.

Elucidation of the role of polyubiquitin binding by A20 for inhibition of IKK

To elucidate this non-catalytic mechanism of IKK inhibition, I considered alternative biochemical properties of A20. A20's ZnF motifs share homology to the ZnF motif of Rab5 guanine nucleotide exchange factor (RABEX-5), which was previously shown to bind ubiquitin (Lee et al., 2006; Mattera et al., 2006; Penengo et al., 2006). To assess whether A20 binds to polyubiquitin chains, I mixed partially purified Flag-A20 with K63 polyubiquitin chains synthesized by TRAF6 and UBC13/UEV1A in which some of the ubiquitin has an HA tag, then performed Flag immunoprecipitation followed by HA immunoblotting. A mutant lacking the ovarian tumor domain (ΔOTU), but not one lacking the seven ZnF motifs (ΔZnF), bound to polyubiquitin chains as well as A20 WT (Figure 3.4A, B). To identify specific ZnFs involved in polyubiquitin binding, mutants lacking one or more ZnFs (ZnF 2-7, 3-7, 4-7, 5-7, 6-7, 1-6, 1-5, and 1-4) were tested. Interestingly, multiple ZnFs contributed to polyubiquitin binding, and a substantial binding defect was observed in a mutant lacking only ZnF7 (Figure 3.4C).

Co-crystallization of the ZnF motif of RABEX-5 with ubiquitin revealed ZnF residues that interact with ubiquitin, including Tyr 26 and Gly 27(Lee et al., 2006; Mattera et al., 2006; Penengo et al., 2006). I mutated the corresponding A20 ZnF7 residues Phe 770 and Gly 771, or the highly conserved Cys 779 and Cys 782, to Ala, and compared them to A20 WT or ΔZnF7.

A20 ΔZnF7, C779A/C782A, and F770A/G771A had an equally severe impairment in polyubiquitin binding (Figure 3.4D). Importantly, each of these mutants was defective in IKK inhibition in S100 (Figure 3.4E), suggesting that ZnF7's contribution to polyubiquitin binding is important for IKK inhibition in vitro.

To assess the contribution of the catalytic Cys 103 residue, and of ZnF7-dependent polyubiquitin binding for IKK inhibition in cells, A20 and mutants thereof were expressed in $A20^{-/-}$ murine embryonic fibroblasts (MEFs) via retrovirus. Retroviral expression of A20 WT or C103A limited IL-1β-induced IKK activation to a level similar to that observed in wild type ($A20^{+/+}$) MEFs. By contrast, A20 F770A/G771A was defective in IKK inhibition (Figure 3.5A, B). Similarly, for TNFα-induced IKK activation, expression of A20 WT or C103A largely rescued A20 function in $A20^{-/-}$ MEFs, while A20 F770A/G771A was defective (Figure 3.6A, B). Thus, in MEF cells, Cys 103 is dispensable for limiting IKK activation within the first few minutes of ligand detection, while ZnF7-dependent polyubiquitin binding is important.

While this work was in progress, it was reported that A20 ZnF4 binds to ubiquitin, and that this binding is important for A20's E3 ubiquitin ligase activity and for inhibition of NF-κB (Bosanac et al., 2010). The authors of this report found that mutation of A20 Tyr 614 and Phe 615 to Ala (Y614A/F615A) within ZnF4 caused reduced ability to bind ubiquitin and to downregulate NF-κB. Therefore in subsequent experiments this mutant was also tested for comparison to A20 WT and the A20 ZnF7 mutant (F770A/G771A) that I had created.

To further test the roles of A20 Cys 103 and polyUb binding for NF-κB downregulation in cells, I established stable cell lines wherein A20 WT, C103A, F770A/G771A (ZnF7*), or Y614A/F615A (ZnF4*) were expressed at similar levels in $A20^{-/-}$ MEFs (Figure 3.7A). I then used RT-PCR to measure expression of two NF-κB target genes, interleukin-6 (IL-6) and

Figure 3.4

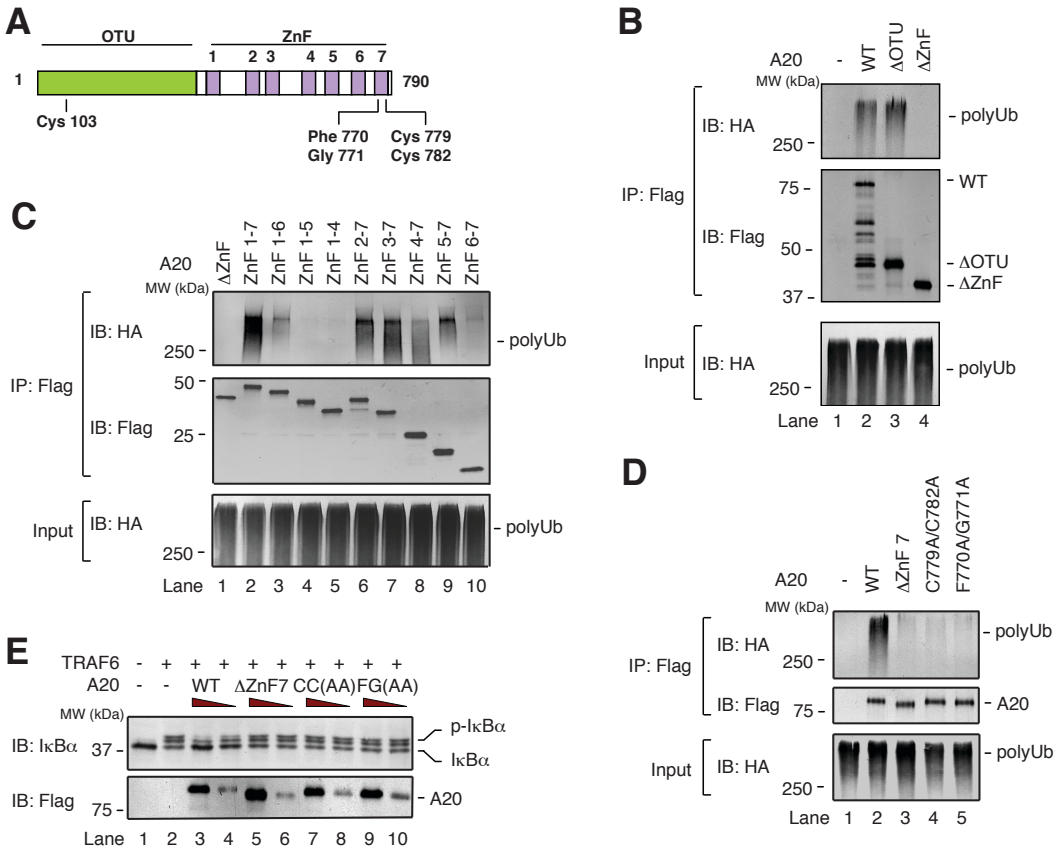

Figure 3.4. Polyubiquitin binding by A20 is largely dependent on ZnF7, and is important for IKK inhibition.

(A) Domain architecture of A20, including relative locations of point mutations. OTU: ovarian tumor. ZnF: zinc finger. (B-D) Flag-A20 mutants were expressed in HEK293 cells and affinity purified. After incubation with HA-tagged polyubiquitin chains, A20 proteins were immunoprecipitated with a Flag antibody and ubiquitin chains were detected by immunoblotting with an HA antibody. (E) IKK activation was measured as in Figure 2.3B. CC(AA): C779A/C782A. FG(AA): F770A/G771A.

Figure 3.5

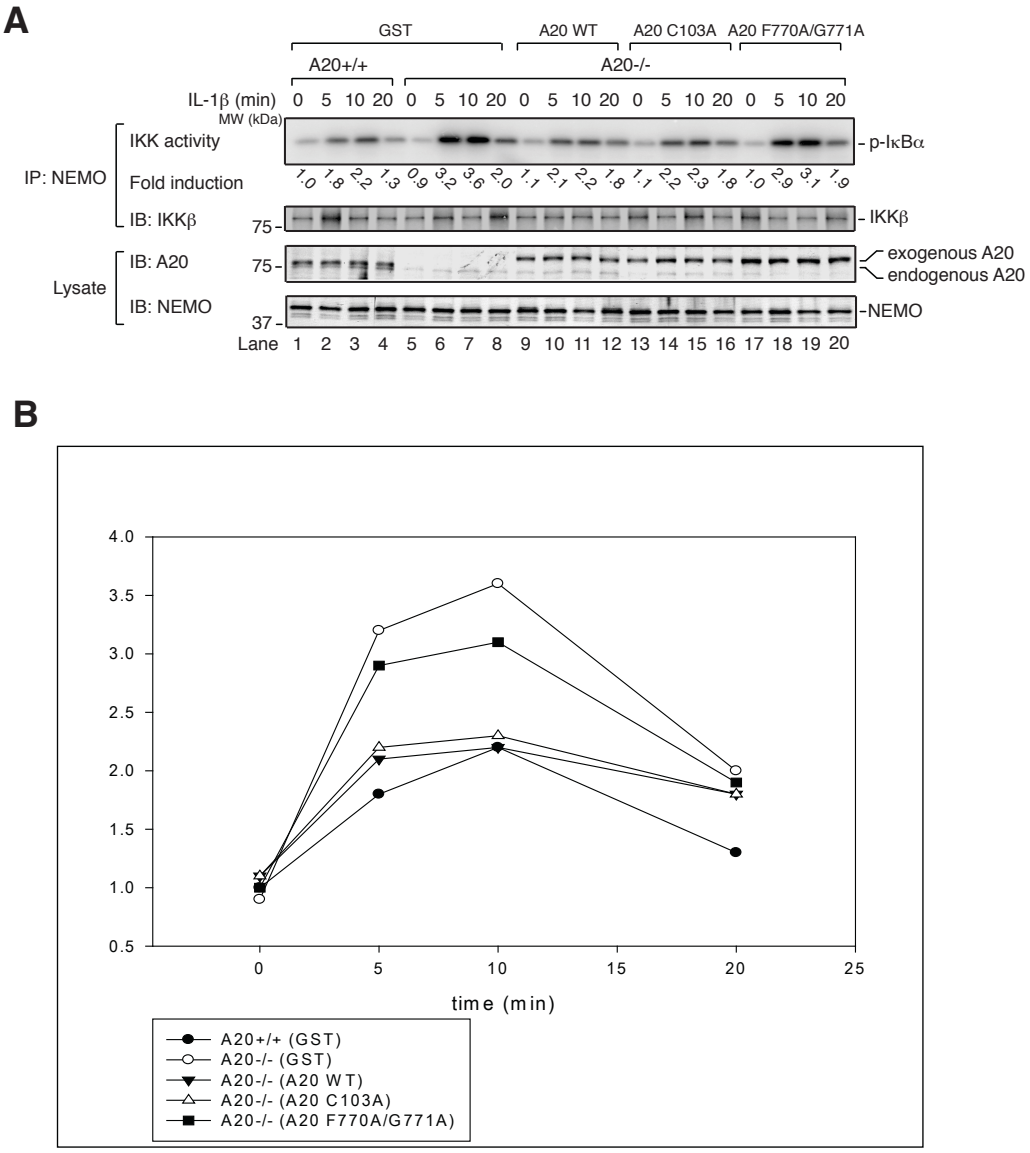

Figure 3.5. A20 Cys 103 is dispensable, while ZnF7-dependent polyubiquitin binding is important for IKK inhibition in the IL-1β signaling pathway.
(A) A20+/+ or -/- MEF cells were infected with retrovirus expressing GST or Flag-A20 WT, C103A, or F770A/G771A. The cells were stimulated with IL-1β for the indicated times, and IKK activity was measured as in Figure 3.1A. Fold activation indicates activity normalized to the activity of unstimulated A20+/+ cells (lane 1). (B) Graphical representation of fold activation data from (A).

Figure 3.6

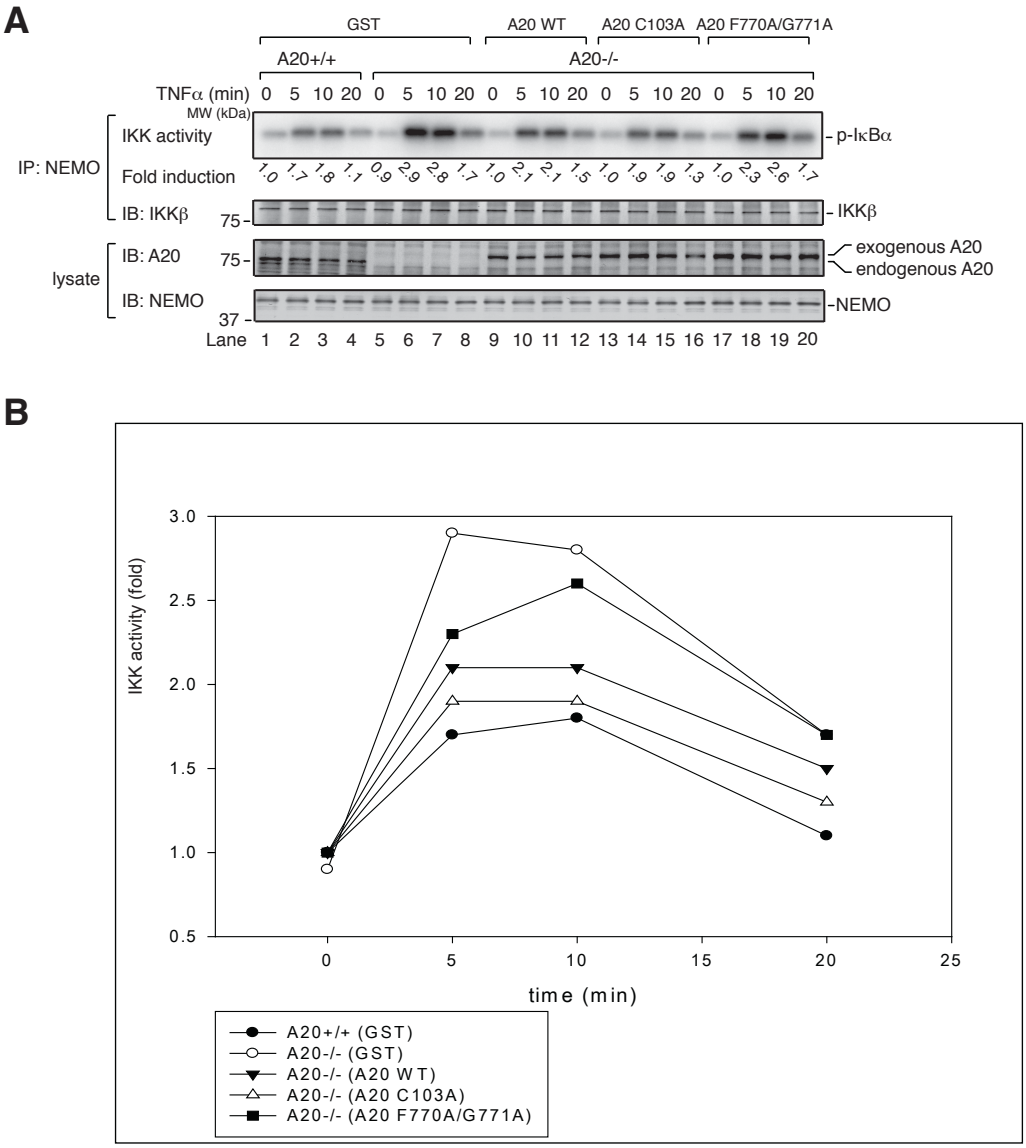

Figure 3.6. A20 Cys 103 is dispensable, while ZnF7-dependent polyubiquitin binding is important for IKK inhibition in the TNFα signaling pathway.
(A) A20+/+ or -/- MEF cells were infected with retrovirus expressing GST or Flag-A20 WT, C103A, or F770A/G771A. The cells were stimulated with TNFα for the indicated times, and IKK activity was measured as in Figure 3.1A. Fold activation indicates activity normalized to the activity of unstimulated A20+/+ cells (lane 1). (B) Graphical representation of fold activation data from (A).

cyclooxygenase-2 (COX-2) before or after stimulation of these cells for 3 hr with TNFα. Not surprisingly, $A20^{-/-}$ MEFs expressing GFP as a control had much higher levels of IL-6 and COX-2 mRNA than $A20^{+/+}$ MEFs expressing GFP, and expression of A20 WT largely suppressed IL-6 and COX-2 expression (Figure 3.7B). Expression of IL-6 and COX-2 in cells with A20 C103A was higher than what was observed in cells with A20 WT, but substantially less than that in cells with GFP. This suggests that downregulation of NF-κB by A20 is partially, but not completely dependent on Cys 103. Importantly, IL-6 and COX-2 expression was significantly elevated in cells expressing either A20 ZnF7* or ZnF4*, confirming the key role of polyUb binding for suppressing NF-κB activity.

Importantly, no change was seen in the abundance of RIP1, UBC13, or UBC5 over the three-hour TNFα treatment regardless of whether A20 WT or mutants were expressed (Figure 3.7C). Thus, over this time period, A20 did not appear to affect the overall stability of these proteins. To see whether TNFα-induced RIP1 ubiquitination was affected by A20 in these cell lines, I immunoprecipitated NEMO from untreated or TNFα-treated cells and immunoblotted for RIP1. $A20^{+/+}$ MEFs and $A20^{-/-}$ MEFs expressing A20 WT appeared to have slightly less high molecular weight RIP1 Ub-conjugates compared to $A20^{-/-}$ MEFs expressing GFP or A20 mutants (Figure 3.7D). This suggests that, in these cells, A20 WT is having some effect on RIP1 ubiquitination status. Nevertheless, A20 WT and C103A each appeared to impair TNFα-induced IKK phosphorylation, whereas the ZnF7 and ZnF4 Ub-binding mutants did not. Therefore RIP1 ubiquitination status appears to be not entirely predictive of IKK activation, i.e., A20 C103A impaired IKK activation even though it did not reduce RIP1 ubiquitination.

Figure 3.7

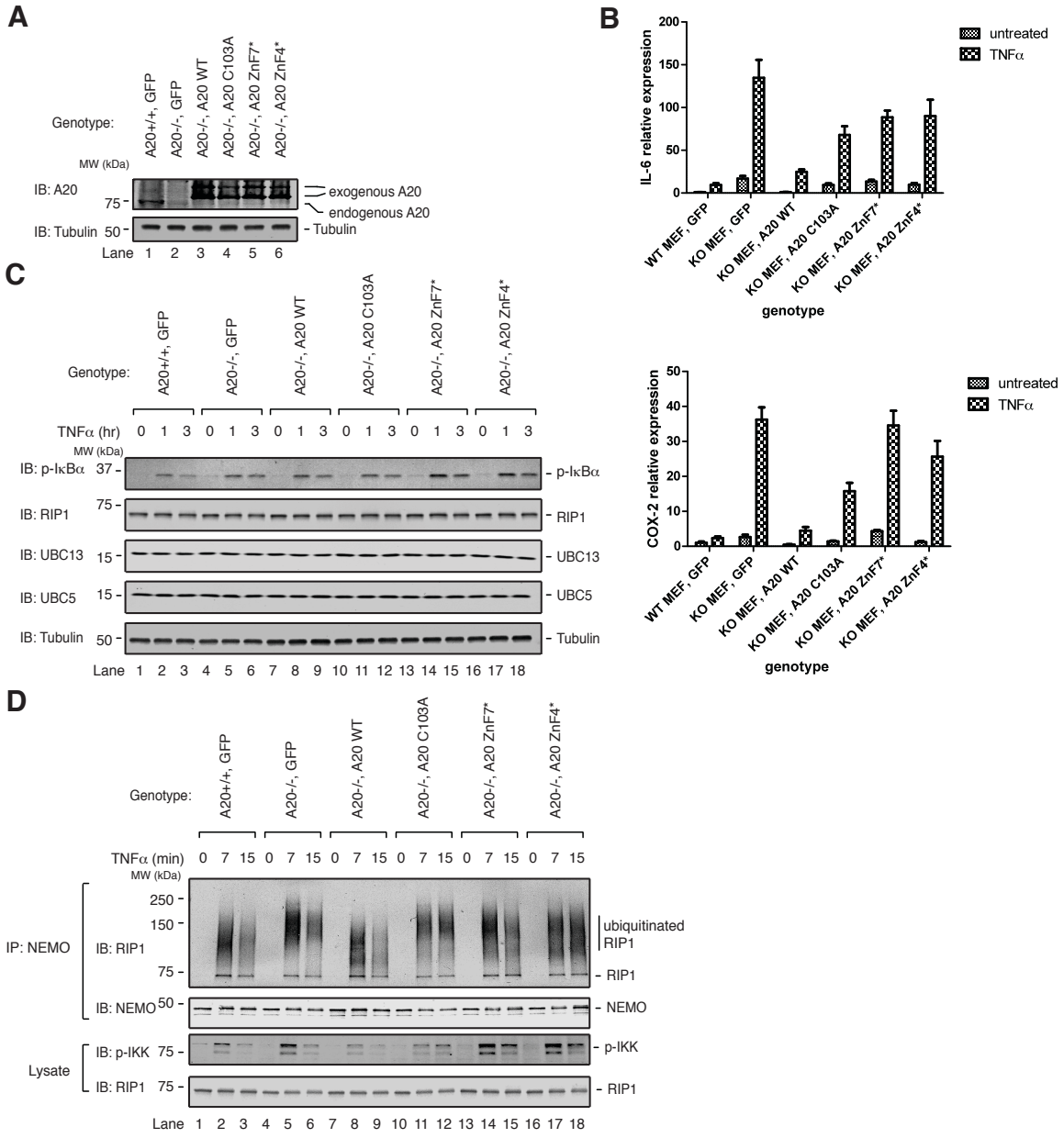

Figure 3.7. The roles of A20's catalytic Cys 103 residue and ubiquitin binding in downregulation of NF-κB activity. (A) Lysates from cells stably expressing GFP or A20 WT or mutants were examined for A20 expression by immunoblotting. (B) Cells were untreated or treated with TNFa for 3 hr. RNA was extracted, and RT-PCR was performed to measure the relative expression of IL-6 or COX-2 as described in experimental procedures. Error bars indicate the standard error of the mean (SEM) among triplicates for each sample. Each graph is representative of three independent experiments. (C) Cells were treated for the indicated times with TNFa. Cell lysates were immunoblotted with the indicated antibodies. (D) Cells were treated for the indicated times with TNFa. Cell lysates were used for immunoprecipitation with a NEMO antibody. Cell lysates and immunoprecipitates were immunoblotted with the indicated antibodies.

Polyubiquitin-mediated NEMO-A20 interaction

Given A20's ability to non-catalytically impair IKK activation, I wondered about the downstream effects of A20's recruitment to polyubiquitin chains. My thoughts regarding this question were influenced by the results described in the previous section (page…). Specifically, these results led to the hypothesis that NEMO and A20 might interact in a stimulus-dependent manner. In addition, NEMO and A20 were previously found to interact in a yeast two-hybrid screen and when overexpressed in mammalian cells (Zhang et al., 2000). Interestingly, I found that endogenous NEMO and A20 co-immunoprecipitated following IL-1β stimulation of HeLa cells with kinetics that correlated with IKK activity (Figure 3.8A). Similarly, TNFα stimulation of HEK293 cells induced interaction between NEMO and A20, concomitant with IKK activation (Figure 3.8B). This correlation suggested that IKK might promote NEMO-A20 interaction, which could explain how phosphorylation of A20 by IKK promotes NF-κB suppression (Hutti et al., 2007). However, as was the case with the TAX1BP1-A20 interaction, the IKK inhibitor TPCA-1 enhanced TNFα-induced NEMO-A20 interaction (Figure 3.8B, lanes 5-8), suggesting that the kinase activity of IKK impairs NEMO-A20 interaction, while an alternative signal induces it. To identify this signal, NEMO-A20 interaction was examined in S100. The combination of TRAF6 and TPCA-1, or an alternative IKK inhibitor BMS-345541, induced NEMO-A20 interaction (Figure 3.9A, B). Addition of the deubiquitination enzyme vOTU abolished this interaction (Figure 3.9C, compare lanes 3 & 6). Depletion of UBC13 from S100 also abolished NEMO-A20 interaction, which was rescued by adding back recombinant His_6-Ubc13 (Figure …; compare lanes 9 & 12). Thus, TRAF6/UBC13-synthesized polyubiquitin chains induce NEMO-A20 interaction. In support of this notion, A20 WT, but not the polyubiquitin-binding mutant F770A/G771A, co-immunoprecipitated with NEMO from S100 in

Figure 3.8

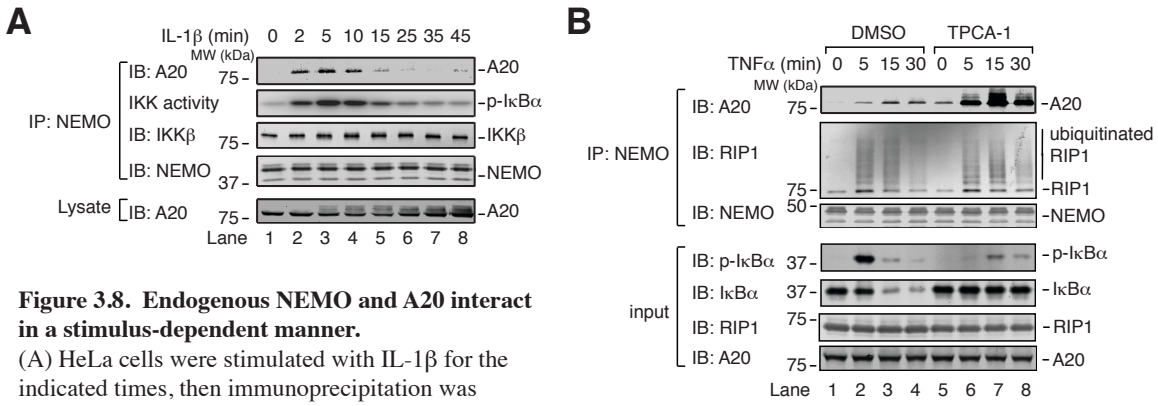

Figure 3.8. Endogenous NEMO and A20 interact in a stimulus-dependent manner.
(A) HeLa cells were stimulated with IL-1β for the indicated times, then immunoprecipitation was performed with a NEMO antibody. Immunoprecipitate was used for measurement of IKK activity as in Figure 3.1A. Lysates and immunoprecipitate were also used for immunoblotting with the indicated antibodies. (B) HEK293 cells were treated with TPCA-1 (10 μM) or an equivalent volume of DMSO for 3 hr. Cells were then treated with TNFα for the indicated times, and a NEMO antibody was used for immunoprecipitation. Cell lysate and immunoprecipitate were immunoblotted with the indicated antibodies.

a TRAF6-dependent manner (Figure 3.9D). NEMO's interaction with A20 was selective, because under the same conditions it did not interact with the proteasomal subunit S5A, which also bound to polyubiquitin chains (Figure 3.9E).

I next wanted to examine NEMO-A20 interaction in human osteosarcoma cells (U2OS) in which ubiquitin is knocked down by tetracycline-inducible shRNA, and replaced with tetracycline inducible RNAi-resistant WT or K63R Ub (Xu et al., 2009). However, I was unable to detect NEMO-A20 interaction in the absence of IKK inhibitor (data not shown). Therefore TPCA-1 was used to enhance NEMO-A20 interaction. In the presence of TPCA-1, IL-1β-induced interaction between NEMO and A20 was higher in cells expressing WT Ub than in cells expressing the K63R mutant (Figure 3.10A), indicating that K63 polyubiquitination provides a signal for NEMO-A20 interaction in cells.

Furthermore, using the stable MEF cell lines described above, I found that A20 WT, but not the ZnF7 or ZnF4 Ub-binding mutants, co-immunoprecipitated with NEMO following TNFα stimulation (Figure 3.10B). This result strongly suggests that polyubiquitin binding by A20 facilitates its recruitment to NEMO in cells.

Polyubiquitin chains can directly and non-covalently induce NEMO-A20 binding

There are several potential explanations for how polyubiquitin chains could induce NEMO-A20 interaction. In principle, one or both proteins might be covalently modified with ubiquitin. Alternatively, the polyubiquitin chains might promote interaction through non-covalent binding to NEMO and A20. The results in Figure 3.10 also do not distinguish between whether polyubiquitin chains directly induce NEMO-A20 interaction, or, whether other factors are required.

Figure 3.9

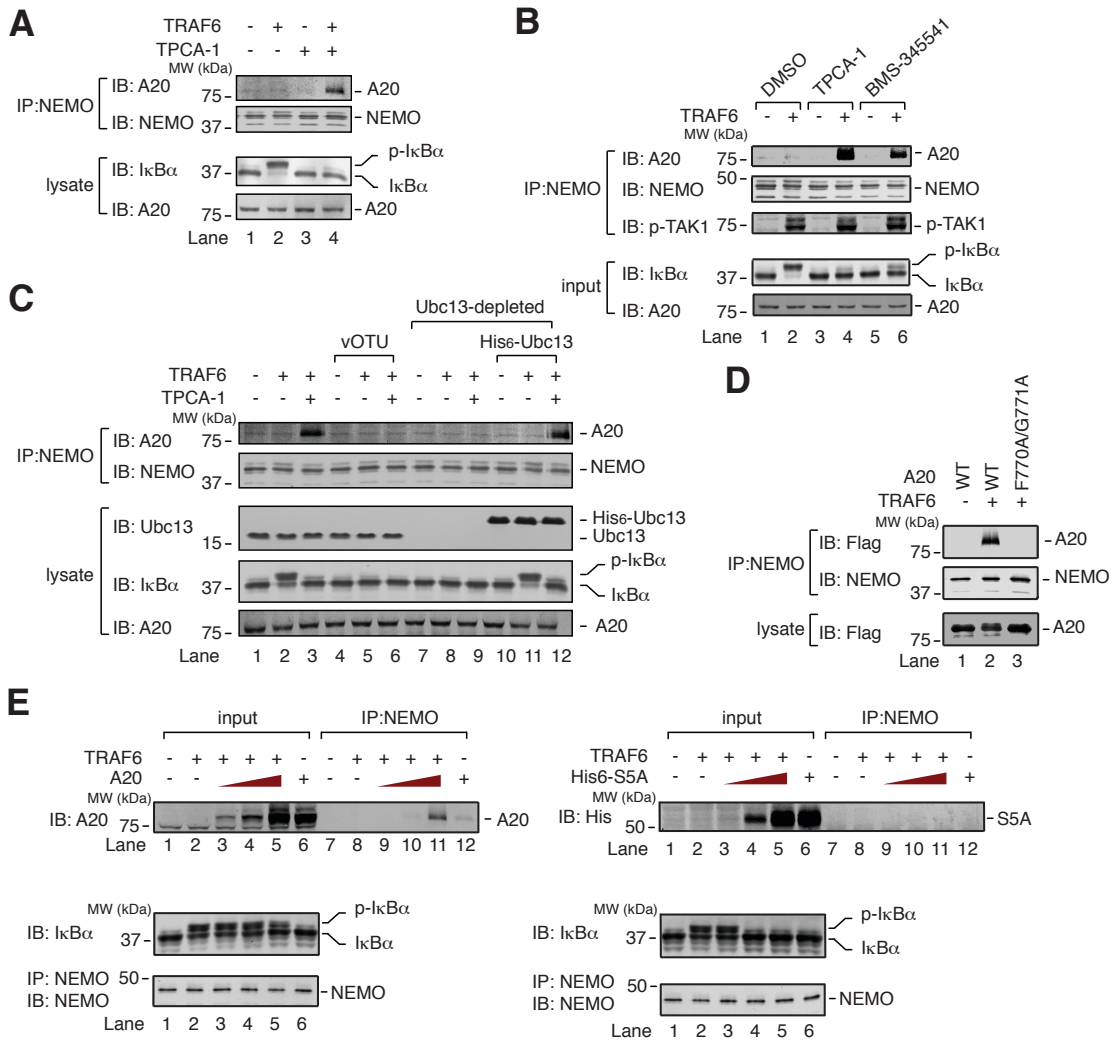

Figure 3.9. Regulation of NEMO-A20 interaction by IKK and polyubiquitin chains.
(A) HeLa cytosolic extract was incubated with ATP, -/+ TRAF6, -/+ TPCA-1 (10 μM) for 1 hr. A NEMO antibody was used for immunoprecipitation. Extract and immunoprecipitate were immunoblotted with the indicated antibodies. (B) As in (A), except that an alternative IKK inhibitor, BMS-345541 (100 μM) was used as well. (C) As in (A), following depletion of UBC13 and/or addition of vOTU or His6-UBC13. (D) A20 WT or F770A/G771A was added to HeLa cytosolic extract. Experiment was performed as in (A), but without TPCA-1. (E) Flag-A20 (left panel) or His6-S5A (right panel) was added to HeLa cytosolic extract with ATP, followed by TRAF6. After 1 hr incubation, 5% of the extract was withdrawn, and the rest was used for immunoprecipitation with a NEMO antibody. Input and immunoprecipitate were immunoblotted with the indicated antibodies. As a control for detection sensitivity, input and immunoprecipitate were run on the same gel. The failure of TRAF6 to induce IkBa phosphorylation in the presence of high S5A concentrations likely indicates that S5A bound to the polyubiquitin chains synthesized by TRAF6, competing with NEMO for polyubiquitin binding.

Figure 3.10

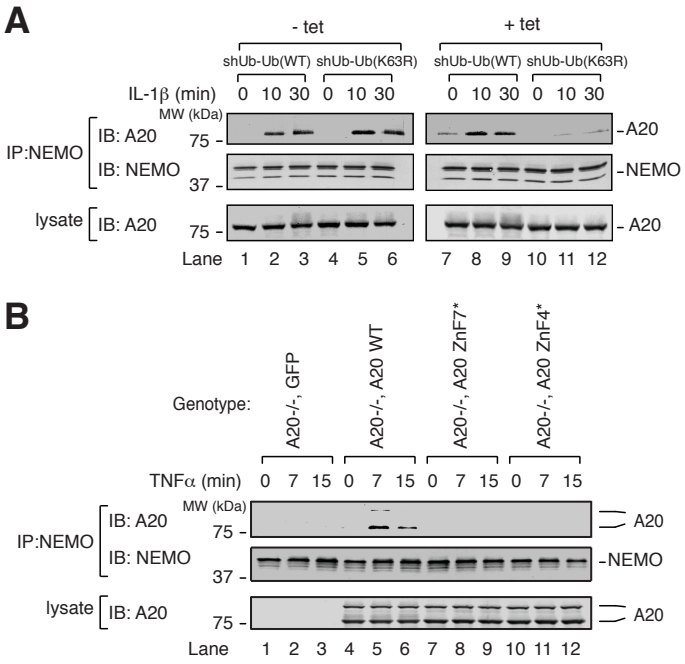

Figure 3.10. Polyubiquitin chains mediate NEMO-A20 interaction in cells.
(A) shUb-Ub (WT) or shUb-Ub (K63R) cells were untreated or treated with tetracycline (1 μg/ml) for 4 days. Cells were then treated with TPCA-1 (20 μM) for 3 hr to enhance NEMO-A20 interaction. Cells were treated with IL-1β for the indicated times, then a NEMO antibody was used for immunoprecipitation. Cell lysates and immunoprecipitates were immunoblotted with the indicated antibodies. (B) MEF stable cell lines were treated for the indicated times with TNFα. Cell lysates were used for immunoprecipitation with a NEMO antibody. Cell lysate and immunoprecipitate were immunoblotted with the indicated antibodies.

To determine if polyubiquitin chains directly promote NEMO-A20 interaction, I incubated highly purified K63 polyubiquitin chains, recombinant GST-NEMO, and A20, then performed GST pull down analyses. These polyubiquitin chains had been synthesized by recombinant E1, UBC13/UEV1A, and TRAF6, each of which was His-tagged. The polyubiquitin chains were subsequently separated from the ubiquitination enzymes by Nickel depletion and gel filtration (Figure 3.11A-C). NEMO and A20 did not detectably interact in the absence of polyubiquitin chains, but robustly interacted in their presence (Figure 3.12A). Importantly, A20 did not impair the interaction between NEMO and polyubiquitin chains, even when A20's molar concentration was roughly 6-fold greater than that of NEMO (lane 8). This result suggests that non-covalent binding to polyubiquitin chains directly induces NEMO-A20 interaction. To confirm that the polyubiqutin chains inducing NEMO-A20 interaction were indeed "free," or unanchored, I treated them with the deubiquitination enzyme Isopeptidase T (IsoT), which is specific for unanchored polyubiquitin chains (Reyes-Turcu et al., 2006). IsoT treatment destroyed the vast majority of polyubiquitin chains, and abolished the NEMO-A20 interaction (Figure 3.12B), supporting the idea that unanchored polyubiquitin chains can induce NEMO-A20 interaction.

Tetraubiquitin of K63-, K48-, or linear linkage did not induce NEMO-A20 interaction, nor did it affect NEMO-A20 interaction in the presence of long polyubiquitin chains (data not shown). It should be noted that, under the experimental conditions used here, NEMO bound to long polyubiquitin chains much more robustly than to tetraubiquitin (data not shown). Therefore, the inability of tetraubiquitin to affect NEMO-A20 binding may simply reflect the relatively low affinity between NEMO and short polyubiquitin chains.

Figure 3.11

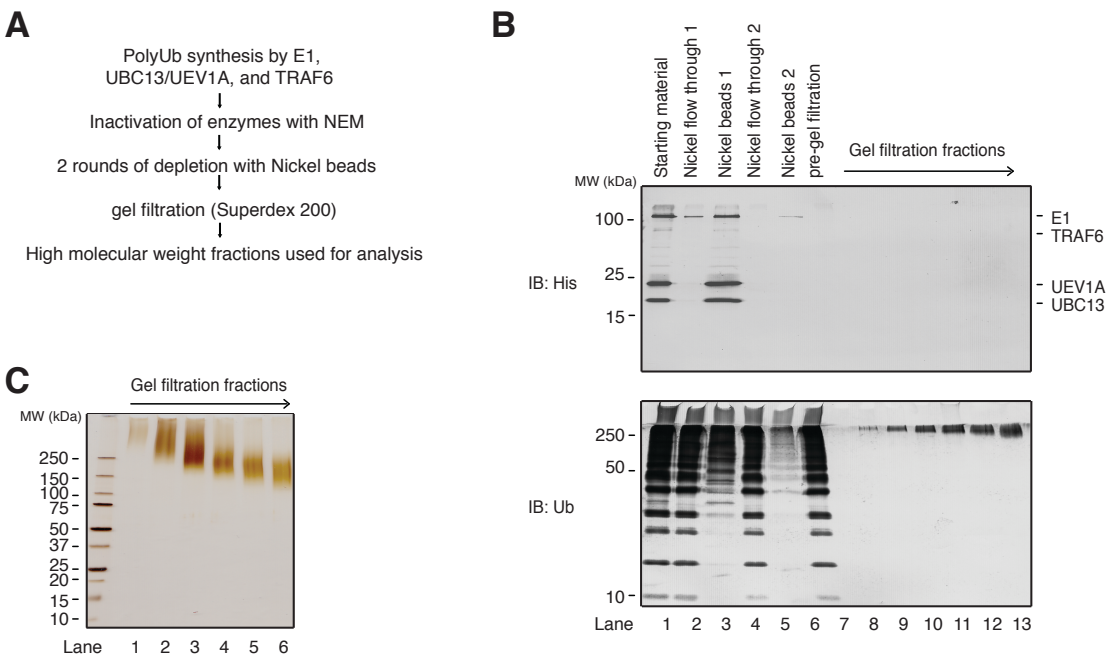

Figure 3.11. Purity of the polyubiquitin chains used for NEMO-A20 binding assays.
(A) Flow chart summarizing method for synthesis and purification of polyubiquitin chains. (B) An aliquot from each step of the polyUb purification was analyzed by immunoblotting with the indicated antibodies. (C) High molecular weight fractions from gel filtration were analyzed by silver staining.

Figure 3.12

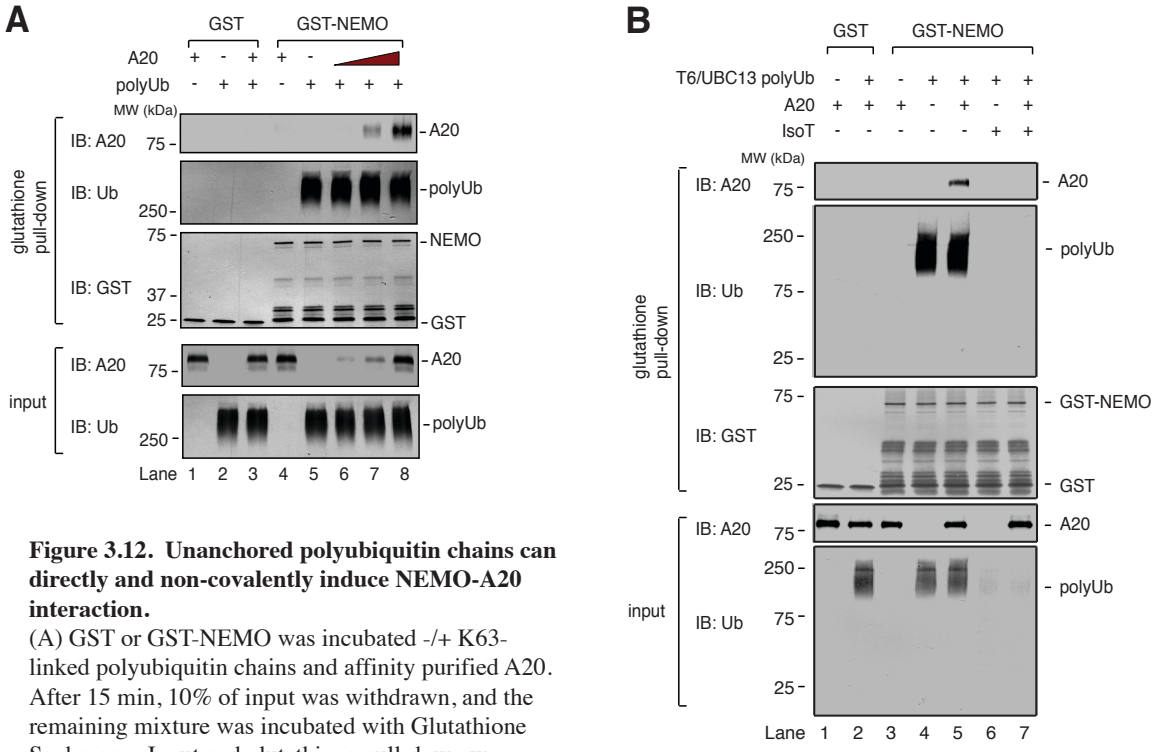

Figure 3.12. Unanchored polyubiquitin chains can directly and non-covalently induce NEMO-A20 interaction.
(A) GST or GST-NEMO was incubated -/+ K63-linked polyubiquitin chains and affinity purified A20. After 15 min, 10% of input was withdrawn, and the remaining mixture was incubated with Glutathione Sepharose. Input and glutathione pull-down were immunoblotted with the indicated antibodies. (B) As (A), but some of the polyubiquitin chains (lanes 6-7) were first treated with IsoT.

In a yeast two-hybrid screen, it was found that A20's interaction with NEMO required a region of NEMO encompassing residues 95-218, which includes its first coiled coil domain (Zhang et al., 2000). On the other hand, polyubiquitin chains bind to NEMO's C-terminus, which contains two ubiquitin binding domains in tandem (Ea et al., 2006; Laplantine et al., 2009; Wu et al., 2006). This suggests that distinct regions of NEMO mediate interaction with A20 and polyubiquitin chains. To test this idea, I purified a fragment of NEMO lacking the first coiled coil domain but containing the ubiquitin-binding domains (251-419, or, NEMO ΔN). NEMO ΔN did not bind A20 even in the presence of polyubiquitin chains (Figure 3.13A, lanes 7-9). In fact, A20 reduced the binding of NEMO ΔN to polyubiquitin chains (lane 9), suggesting that A20 and NEMO ΔN compete for polyubiquitin binding, whereas A20 and full-length NEMO cooperate to form a ternary complex in the presence of polyubiquitin. The formation of this complex involves not only the binding of NEMO and A20 to polyubiquitin chains, but also a domain within NEMO's N-terminus, presumably because this domain interacts directly with A20 (Figure 3.13B). If this complex involves direct interaction between NEMO and A20, it is expected that other polyubiquitin-binding proteins will not bind to NEMO under these conditions, assuming they lack an interface for binding to NEMO. Indeed, interaction was not detected between NEMO and recombinant TAB2 in the presence or absence of polyubiquitin chains; rather, TAB2 at high concentration appeared to compete with NEMO for binding to polyubiquitin chains (Figure 3.13C, lane 14). These results suggest that polyubiquitin chains can directly and non-covalently induce specific binding between NEMO and A20 (see discussion).

My effort to identify a region of A20 required for binding to NEMO initially looked promising as well. When added to S100 along with TRAF6 and ATP, A20 WT interacted with endogenous NEMO, whereas deletion mutants lacking either the OTU domain (ΔOTU) or the

Figure 3.13

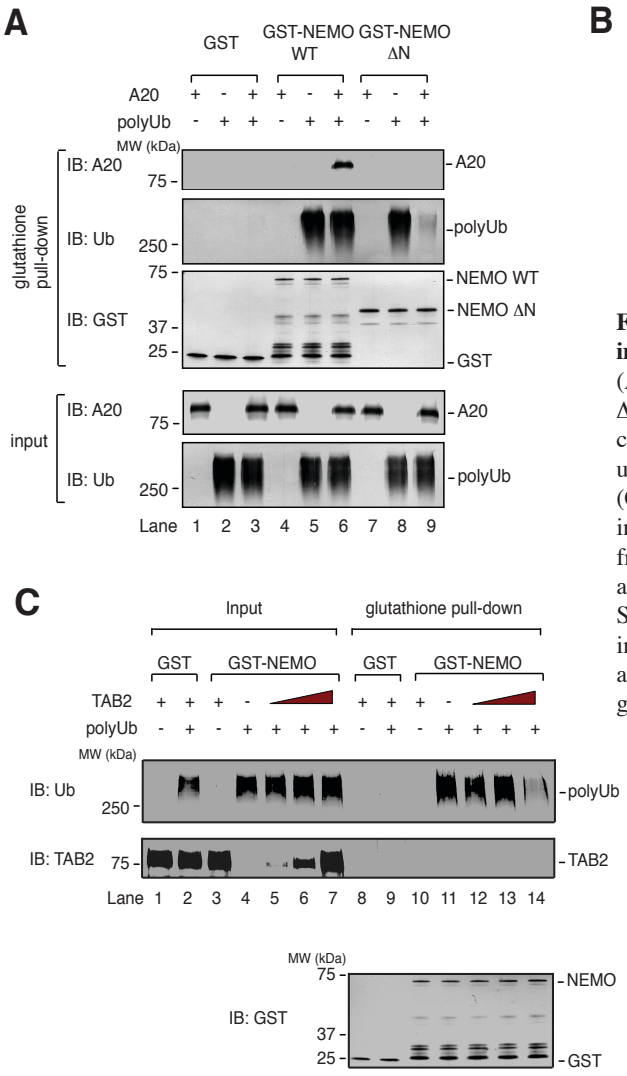

Figure 3.13. Polyubiquitin-induced NEMO-A20 interaction is specific.
(A) As in Figure 3.12A, but including GST-NEMO ΔN. (B) Model of polyubiquitin-NEMO-A20 complex. NT: N-terminus. NUB: NEMO ubiquitin binding. ZnF: zinc finger. Ub: ubiquitin. (C) Recombimant GST or GST-NEMO was incubated -/+ polyubiquitin chains, -/+ His6-TAB2 from SF9 cells. 10% of the input was withdrawn, and the remainder was incubated with Glutathione Sepharose. Input and glutathione pull-down were immunoblotted with the indicated antibodies. As a control for detection sensitivity, input and glutathione pull-down were run on the same gel.

ZnF region (ΔZnF) did not (Figure 3.14A). It is likely that the ΔZnF region fails to interact with NEMO because of its inability to bind to polyubiquitin chains. Given that the OTU region appears not to contribute to polyubiquitin binding, my result suggested that the OTU domain is required for binding to NEMO. Moreover, A20's ability to bind to NEMO correlated with its ability to inhibit IKK. A20 ΔOTU was a less potent inhibitor of IKK in S100 than A20 WT (Figure 3.14B, lanes 4 and 8), while A20 ΔZnF did not inhibit IKK at all (data not shown). To test whether A20's OTU domain is directly involved in binding to NEMO, A20 ΔOTU was purified through the two-step affinity purification method described above, then tested in the assay described in Figure 3.12. Surprisingly, in this assay, A20 ΔOTU bound as well as A20 WT to NEMO in the presence of polyubiquitin chains (Figure 3.14C). Thus, the contribution of A20's OTU domain to NEMO binding appears to be indirect, i.e., mediated by some factor(s) present in cytosolic extract.

Direct, non-catalytic impairment of IKK activation by A20

The signal-induced recruitment of A20 to NEMO suggests that A20 might directly regulate IKK. However, the activity of IKK complex immunoprecipitated from TNFα-stimulated cells was unaffected by A20 (Figure 3.15A). In fact, removal of polyubiquitin chains from NEMO-associated RIP1 by vOTU did not affect IKK activity, whereas dephosphorylation by lambda phosphatase abolished it (Figure 3.15B). Thus, IKK phosphorylation appears to be the primary determinant of its kinase activity.

I then tested whether A20 could prevent IKK phosphorylation, using an assay in which IKK complex is activated by TAK1 in the presence of unanchored K63 polyubiquitin chains (Xia et al., 2009). To uncouple the processes of TAK1 and IKK activation, TAK1 was first activated

Figure 3.14

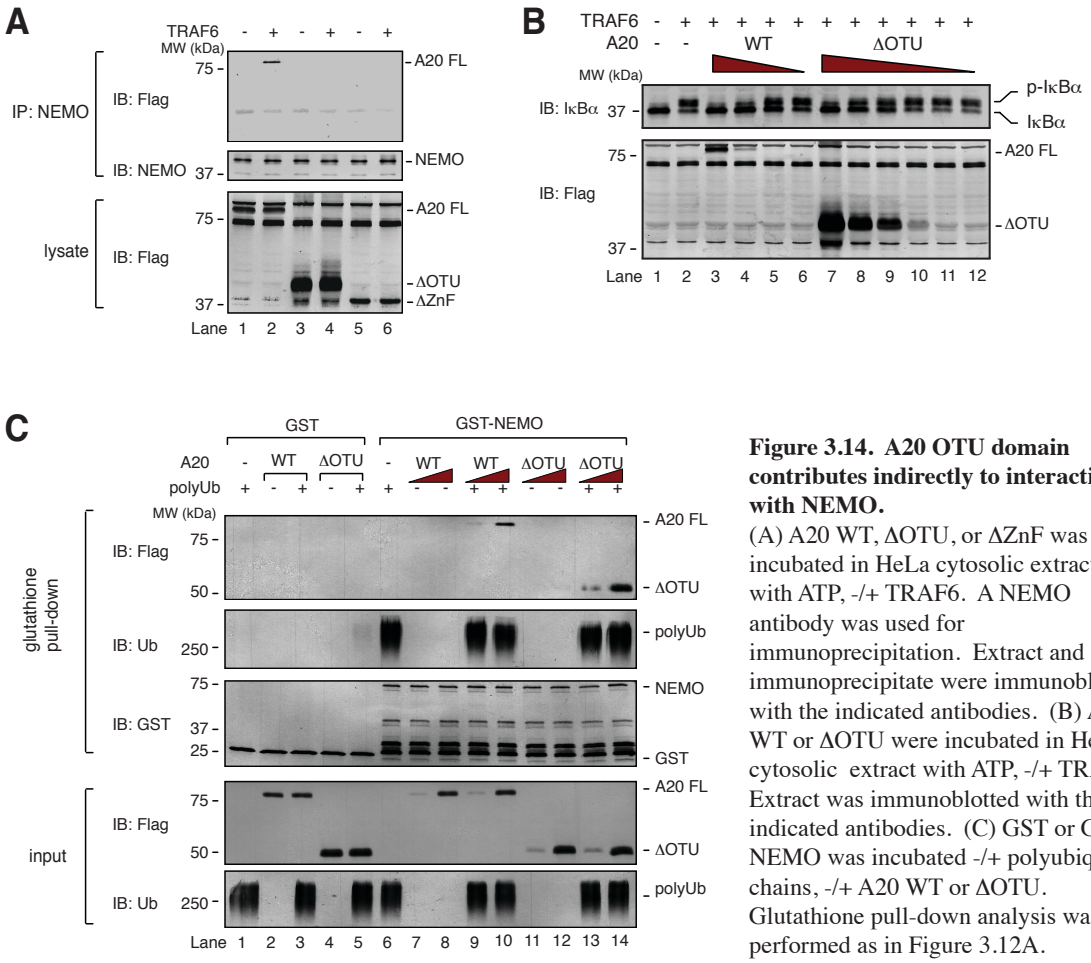

Figure 3.14. A20 OTU domain contributes indirectly to interaction with NEMO.
(A) A20 WT, ΔOTU, or ΔZnF was incubated in HeLa cytosolic extract with ATP, -/+ TRAF6. A NEMO antibody was used for immunoprecipitation. Extract and immunoprecipitate were immunoblotted with the indicated antibodies. (B) A20 WT or ΔOTU were incubated in HeLa cytosolic extract with ATP, -/+ TRAF6. Extract was immunoblotted with the indicated antibodies. (C) GST or GST-NEMO was incubated -/+ polyubiqutin chains, -/+ A20 WT or ΔOTU. Glutathione pull-down analysis was performed as in Figure 3.12A.

Figure 3.15

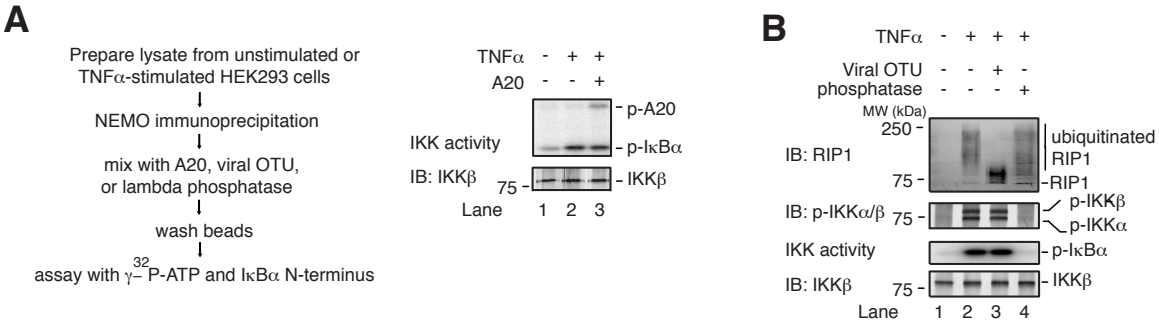

Figure 3.15. A20 did not inactivate IKK.
(A) HEK293 cells were untreated or treated with TNFα for 10 min, and a NEMO antibody was used for immunoprecipitation. Immunoprecipitate was incubated with affinity-purified A20, then washed and incubated with γ-32P-ATP and GST-IκBα N-terminus or immunoblotted with the indicated antibodies. (B) As in (A), but NEMO immunoprecipitate was treated with vOTU or lambda phosphatase.

by polyubiquitin chains, which were subsequently destroyed using vOTU, then the TAK1 complex was affinity purified (Figure 3.16A). Phosphorylation of MKK6 by this constitutively active TAK1 (TAK1-ca) was no longer subject to regulation by polyubiquitin chains (Figure 3.16B, bottom). Interestingly, phosphorylation of IKK by TAK1-ca was significantly enhanced by polyubiquitin chains (Figure 3.16B, top; compare lanes 5 & 6), indicating that polyubiquitin chains are required not only for TAK1 activation, but also for the phosphorylation of IKK by active TAK1. Remarkably, A20 had no effect on phosphorylation of MKK6 by TAK1-ca, but impaired phosphorylation of IKK (Figure 3.16C, top and middle), indicating that A20 can impair IKK phosphorylation without affecting TAK1 activity per se. As a control, phosphorylation of IKK by the kinase MEKK1, which does not require ubiquitin, was unaffected by A20 (Figure 3.16C, bottom). Importantly, A20 C103A impaired IKK phosphorylation as potently as A20 WT, whereas further deletion of ZnF7 attenuated this inhibitory activity (Figure 3.16D). These results provide direct evidence that A20 inhibits IKK by preventing the phosphorylation of IKK by TAK1.

As an additional test that A20's impairment of IKK phosphorylation can occur without any impairment of TAK1 activity, I used an alternative assay for activation of purified IKK complex (Xia 2009). In this assay, IKK is activated in the absence of TAK1 using polyubiquitin chains synthesized by TRAF6 and the E2 enzyme UBC5 (Figure 3.17A). Although the physiological significance of this mechanism of IKK activation is unknown, it provides a way to activate IKK without TAK1, because these polyubiquitin chains induce IKK autophosphorylation. A20 was able to impair IKK phosphorylation in a manner independent of its Cys 103 residue, but largely dependent on ZnF7 (Figure 3.17B), further supporting the idea that A20 binding to NEMO is sufficient to impair IKK activation. The molar ratio of A20 to

Figure 3.16

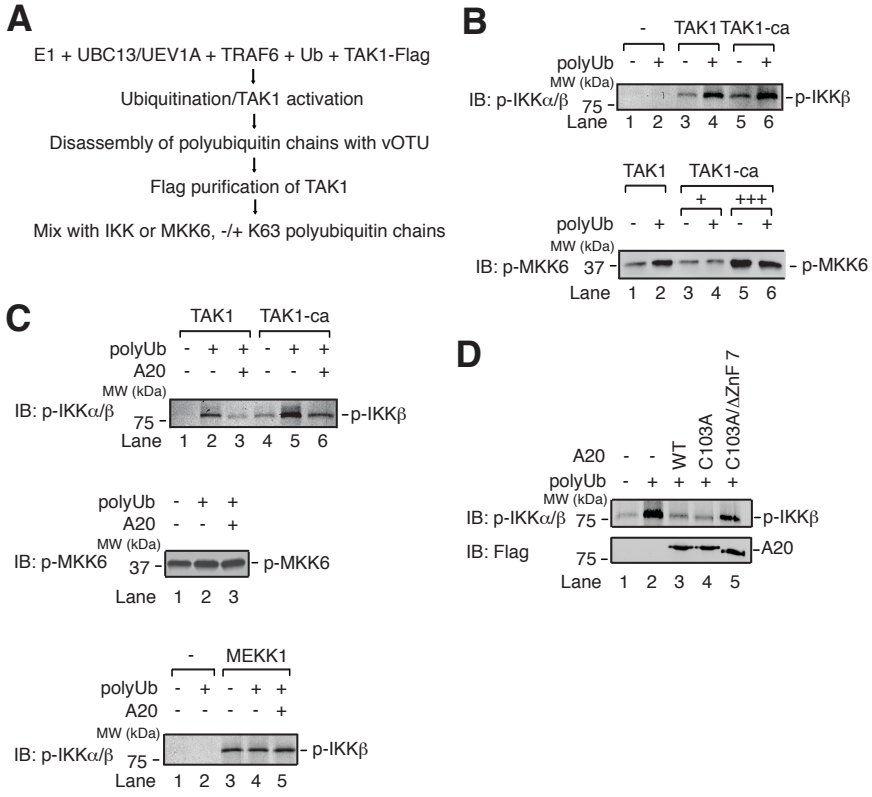

Figure 3.16. A20 can directly and non-catalytically impair IKK phosphorylation by TAK1
(A) Method to generate constitutively active TAK1 (TAK1-ca). (B) top: TAK1 or TAK1-ca was incubated with IKK complex and TAP, -/+ polyubiquitin chains. Samples were immunoblotted for p-IKK. Bottom: TAK1 or TAK1-ca was incubated with His6-MKK6 (K82A) and ATP, -/+ polyubiquitin chains. Samples were immunoblotted for p-MKK6. (C) Top and middle: as in (B), except that A20 was included in the reactions. Bottm: MEKK1 was used to activate IKK. (D) as in (B) top, except that the reactions included A20 WT, C103A, or C103A/ΔZnF7.

NEMO required for significant inhibition was roughly 1:1 (lanes 3-4). Importantly, even at a molar ratio of 5:1, A20 did not impair co-immunoprecipitation of TRAF6-UBC5-synthesized polyubiquitin chains by NEMO (Figure 3.17C).

I also found that A20 can impair TAK1 activation by K63-linked polyubiquitin chains in a manner independent of A20's OTU domain, but dependent on polyubiquitin binding by ZnF7 (Figure 3.18).

Figure 3.17

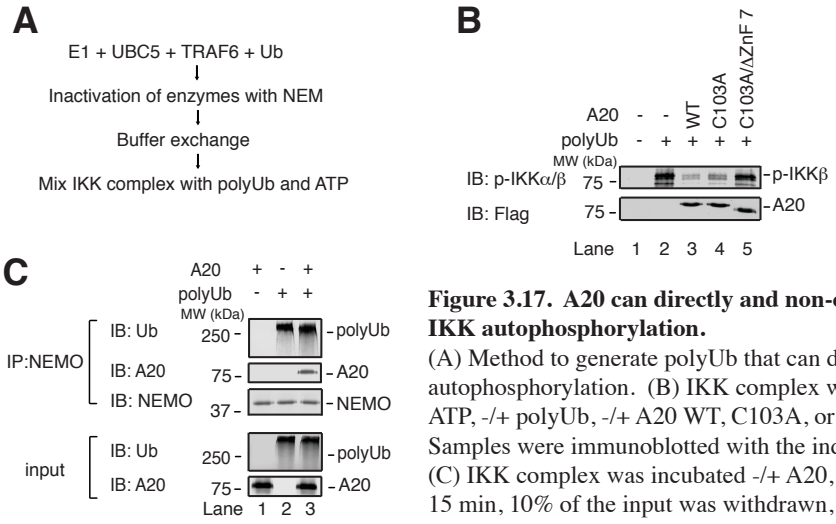

Figure 3.17. A20 can directly and non-catalytically impair IKK autophosphorylation.
(A) Method to generate polyUb that can directly induce IKK autophosphorylation. (B) IKK complex was incubated with ATP, -/+ polyUb, -/+ A20 WT, C103A, or C103A/ΔZnF7. Samples were immunoblotted with the indicated antibodies. (C) IKK complex was incubated -/+ A20, -/+ polyUb. After 15 min, 10% of the input was withdrawn, and the remainder was used for immunoprecipitation with a NEMO antibody. Input and immunoprecipitate were immunoblotted with the indicatd antibodies.

Figure 3.18

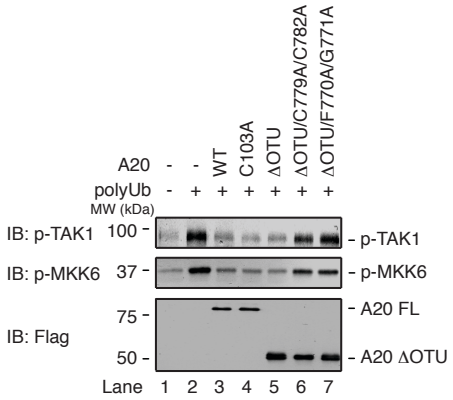

Figure 3.18. A20 can directly and non-catalytically impair TAK1 activation. TAK1 and MKK6 (K82A) were incubated with ATP, -/+ K63-linked polyUb, -/+ A20 WT, C103A, ΔOTU WT, ΔOTU C779/C782A, or ΔOTU F770A/G771A. Samples were immunoblotted with the indicated antibodies.

Discussion

Novel, non-catalytic mechanism of IKK inhibition by A20

My results suggest a mechanism by which A20 inhibits IKK without deubiquitination or impairment of ubiquitination enzymes. I propose that, within the first few minutes of ligand detection, A20 forms a complex with polyubiquitin chains and NEMO and non-catalytically limits the extent of IKK activation by TAK1 (Figure 3.19). Indeed, I present multiple lines of evidence that A20 inhibits IKK through a non-catalytic mechanism. First, when overexpressed, A20 inhibits TNFα-induced IKK activation without impairing ubiquitination of RIP1. Second, in cell-free systems that partially recapitulate the IL-1R signaling pathway, the C103A mutant of A20 is as potent as A20 WT in inhibition of IKK. Finally, A20 C103A impairs activation of IKK when expressed in $A20^{-/-}$ MEFs. My measurements of NF-κB target gene expression suggest that a C103-dependent means of IKK inhibition does play a role in NF-κB downregulation under conditions of sustained stimulation with TNFα. However, the majority of NF-κB downregulation by A20 does not require the catalytic Cys 103 residue. Of course, conclusive evidence regarding the role of A20 Cys 103 in IKK inhibition and control of inflammation will require analysis of a knock-in mouse harboring mutation of this residue.

My results suggest that multiple A20 ZnFs contribute to polyubiquitin binding, including a prominent contribution by ZnF7. Consistent with a key role for ZnF7, mutations in this motif that impair polyubiquitin binding reduce A20's ability to inhibit IKK in vitro and in reconstituted $A20^{-/-}$ MEFs. It is noteworthy that among the mutations in the A20 gene (*TNFAIP3*) identified in B-cell lymphoma patients, the majority results in premature stop codons or frameshifts that

Figure 3.19

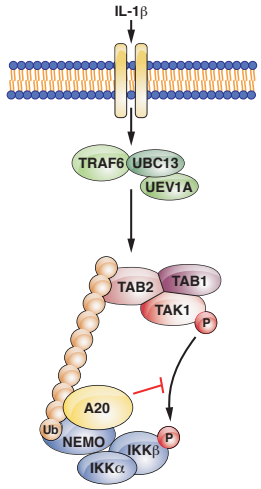

Figure 3.19. A model of the non-catalytic mechanism by which A20 limits IKK activation. Binding of IL-1β to IL-1R activates the E3 ligase TRAF6, which works with UBC13/UEV1A to synthesized K63-linked polyubiquitin chains. The TAK1 and IKK complexes are recruited through ubiquitin binding domains on TAB2 and NEMO, respectively, allowing IKK phosphorylation by TAK1. A20 is recruited to NEMO through bipartitie binding to polyubiquitin chains and an N-terminal region of NEMO. Formation of the complex impairs IKK phosphorylation by TAK1, thereby limiting the extent of IKK activation.

preclude synthesis of some or all of the ZnFs (Compagno et al., 2009; Kato et al., 2009; Schmitz et al., 2009). Although their locations vary widely, almost all of these mutations occur prior to ZnF7. My results suggest that each of these mutations causes a polyubiquitin-binding defect, which is sufficient to cause IKK dysregulation, although other biochemical properties of A20 affected by the mutations should be investigated.

My results indicate that an outcome of polyubiquitin binding by A20 is its recruitment to NEMO. Binding between A20 and NEMO was initially reported more than a decade ago (Zhang et al., 2000), but the relevance of this interaction, and its potential regulation, have not been clearly defined. I found that A20 is recruited to NEMO by polyubiquitin chains, and when bound, can impair IKK activation. Thus, NEMO can receive both positive and negative IKK-regulatory signals.

My data regarding the mechanism by which A20 impairs IKK activation present on the one hand a straightforward and clear model—it seems easy to understand that impaired phosphorylation of IKK impairs its ability to phosphorylate IκBα. On the other hand, the basis for this impaired IKK phosphorylation is unclear. How does binding of A20 to the NEMO-polyUb complex impair phosphorylation of IKK? My data present no obvious answer to this question. In this regard, I believe my data highlight a deficiency in the current understanding of how IKK is regulated by polyubiquitin chains in the first place. For example, there is currently no clear answer to the related question: How does polyubiquitin binding by NEMO facilitate IKK phosphorylation? There seem to be two likely possibilities: polyUb binding by NEMO (1) causes a conformational change in the IKK complex that exposes IKK's phosphorylation site, or, (2) brings IKK complex into proximity with TAK1 complex (or more IKK complex in the case of autophosphorylation). Regarding the conformational change hypothesis, it was reported that,

following stimulation of cells with TNFα, the IKK complex forms a structure large enough to elute in earlier fractions on a Superose 6 gel filtration column compared to IKK complex from unstimulated cells (Poyet et al., 2000). The relevance of this apparent structural change is unknown though. In addition, using similar conditions and materials, I was unable to reproduce this result (data not shown).

In any case, it seems plausible that the binding of A20 to the NEMO-polyUb complex could impair either a necessary conformational change in the IKK complex or its alignment with the TAK1 complex. It is likely that structural characterization of the processes of polyUb-dependent TAK1 and IKK activation, and their inhibition by A20, will be required to gain a detailed understanding of the mechanisms of TAK1 and IKK regulation. In this regard, I began work aimed at elucidating, via electron microscopy, the mechanism of TAK1 activation by polyUb. This work was done in collaboration with Dr. Qui-Xing Jiang in the Department of Cell Biology. 2 μl of two-step affinity-purified TAK1 complex (Figure 2.2A, middle panel) was negatively stained, and viewed with a Tecnai G2 Spirit BioTWIN transmission electron microscope. >5000 particles were manually picked from the images, and correction for contrast transfer function (CTF) was performed. However, at this point, our collaborator chose not to pursue the project further.

It is noteworthy that two oncoproteins have been reported to bind to an N-terminal region of NEMO that overlaps with the region required for NEMO-A20 interaction. The human T cell leukemia virus (HTLV-1) and Kaposi's Sarcoma Herpes virus (KSHV) are both oncogenic viruses known to promote constitutive NF-κB activity. Both the HTLV-1 oncoprotein TAX and the KSHV oncoprotein vFLIP bind to NEMO and promote IKK activation (Bagneris et al., 2008; Field et al., 2003; Fu et al., 2003; Hong et al., 2007). As with polyubiquitin binding to NEMO's

C-terminus, the structural basis for IKK activation via NEMO-TAX or NEMO-vFLIP binding is a mystery. The overlap between the region of NEMO that binds to TAX and vFLIP with the region required for binding to A20 suggests a potential competitive basis for IKK regulation by TAX and vFLIP, e.g., these proteins might impair recruitment of A20 to NEMO, thereby blocking negative regulation. This might be an interesting future direction to pursue.

Consistent with what was reported by Wertz et al. (2004) and Bosanac et al. (2010), I have found that A20's C-terminal ZnF region can catalyze polyUb synthesis in the presence of E1 and UBC5, and this activity was impaired by mutation of ZnF4 (Figure 3.20, lanes 2 and 4). Interestingly, this activity was also impaired by mutation of ZnF7 (F770A/G771A) (lanes 2 and 3). This result suggests an unexpected role for ZnF7 Ub binding in A20's E3 ligase activity. Because these ZnF7 and ZnF4 mutations also impair A20's recruitment to NEMO following TNFα detection (Figure 3.10B), it is difficult to delineate the cause of impaired NF-κB downregulation by the A20 ZnF7 and ZnF4 mutants in vivo. Given the ability of A20 to directly impair IKK phosphorylation when bound to NEMO in vitro, as well as the rapid recruitment of A20 to NEMO that correlates with IKK inhibition in cells, I think it is likely that direct, non-catalytic impairment of IKK activation plays an important role. It is also important to note that that I did not detect an A20-dependent decrease in the stability of RIP1, UBC13, or UBC5 in the time periods I examined (Figure 3.7C). Nevertheless, I cannot rule out a role for A20 E3 ligase activity in downregulation of NF-κB in vivo.

A previous study showed that A20 is recruited to E2-E3 ubiquitination enzymes such as UBC13 and TRAF6, leading to disruption of the E2-E3 interaction (Shembade et al., 2010). This recruitment, which is dependent on A20 Cys 103, appears to occur after IKK activity has declined from its peak, and may therefore serve to further reduce IKK activity towards its basal

Figure 3.20

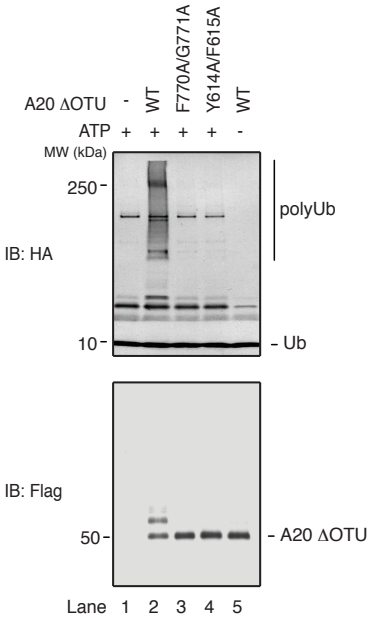

Figure 3.20. A20 ZnF7 and ZnF4 polyUb binding mutants have impaired E3 Ligase activity.
HA-ubiquitin, E1, and UBC5 were incubated -/+ ATP, -/+ A20 ΔOTU WT, F770A/G771A, or Y614A/F615A for 30 min. Samples were immunoblotted with the indicated antibodies.

level and to desensitize the pathway to additional upstream stimulation. However, I was unable to detect stimulus-dependent interaction between TRAF6 and UBC13, or between TRAF6 and A20 (data not shown), making it difficult to test this hypothesis.

A basis for specificity in ubiquitin-mediated signal transduction

I have identified a complex between K63 polyubiquitin chains, A20, and NEMO. Remarkably, the ubiquitin binding domain of NEMO is insufficient for complex formation. Rather, the N-terminus of NEMO is required, presumably because it makes direct contact with A20. A ternary complex of a similar nature was previously described (Kang et al., 2007). In this case, one UIM domain of the proteasome subunit S5A binds to the ubiquitin-like domain of RAD23, while the other UIM domain of S5A and the UBA domain of RAD23 bind to a K48-linked polyubiquitin chain. This interaction may facilitate delivery of K48 polyubiquitin chains into the proteasome. To my knowledge, my results provide the first demonstration of this type of complex in the context of signal transduction. Importantly, this interaction can be achieved with polyubiquitin chains that are not attached to a target protein, such as those synthesized by TRAF6 and UBC13/UEV1A. Thus, non-degradative polyubiquitin chains are sufficient to induce specific protein-protein interaction. Of course, polyubiquitin chains attached to a substrate, such as RIP1, could also mediate this type of interaction.

Previous studies on the role of ubiquitin in signal transduction hint at the possibility that the activities of multiple proteins might be coordinated by their simultaneous recruitment to polyubiquitin chains. For example, simultaneous binding of TAB2 and NEMO to a polyubiquitin chain seems like the most plausible means of promoting IKK activation by TAK1. Yet I am unable to detect interaction between TAB2 and NEMO (Figure 3.13C). Indeed, under

standard conditions for pull-down assays, polyubiquitin binding by two proteins appears insufficient to detect their interaction with each other. It remains likely that polyubiquitin chains organize multi-protein complexes, e.g., TAK1 and IKK complexes, without inducing interactions stable enough for detection in crude pull-down assays. However, my findings suggest a highly specific mode of interaction in which direct contact between ubiquitin binding proteins yields a stable ternary complex. This mode of interaction may help to account for the specific signaling outputs achieved by polyubiquitin chains in diverse cellular pathways.

Additional results and discussion regarding regulation of A20 by IKK and E3 ubiquitin ligases

Given the essential function of A20 as an IKK inhibitor, the impaired recruitment of A20 by IKK at first appears to be a paradox. If A20 must ultimately downregulate IKK, why does IKK block its recruitment? This phenomenon though, along with the knowledge that polyubiquitin chains recruit both activators (TAB2 and NEMO) and an inhibitor (A20) of the NF-κB-regulatory pathways, may be key to tapping into the logic of NF-κB regulation. If no mechanism existed to limit A20 recruitment to NEMO, A20 would presumably be recruited to the same extent as NEMO, thus precluding IKK activation in the first place. This notion is supported by the data that overexpressed A20 does not allow IKK activation by TNFα (Figure 3.1A). Perhaps it should be expected then that, under basal conditions (no overexpression), a mechanism is in place to "tip the balance" towards IKK activation.

To accomplish this feat, IKK might initially phosphorylate A20, leading to impaired recruitment to NEMO. This mechanism might potentially be countered with another mechanism to "overcome" this limitation on recruitment, allowing A20 to be recruited to NEMO and prevent

excess activation. This idea should be considered in the context of other interesting but unexplained phenomena regarding A20, particularly the fact that A20's ability to be recruited to RIP1 and impair IKK activation in vivo depends on the E3 ubiquitin ligases ITCH and RNF11 (Shembade et al., 2008; Shembade et al., 2009). Why are E3 ligases required for A20 to be recruited to its "targets" upstream of IKK? This question led me to a hypothesis that would explain these phenomena in the context of the kinetics of IKK activation and inhibition that occur in the first few minutes of signaling (Figure 3.21). Following synthesis of polyubiquitin chains, NEMO and A20 would be recruited with similar kinetics. However as some IKK activity begins to occur, IKK would phosphorylate A20. This phosphorylation would target A20 to some unknown phospho-A20 binding protein, which would impair A20's interaction with NEMO. Thus, the ratio of NEMO:A20 localized to the polyubiquitin chains would be high, allowing IKK activity to increase. Eventually this phospho-A20 binding protein would be ubiquitinated by ITCH and/or RNF11, targeting it for proteasomal degradation. A20, despite remaining phosphorylated, would now be "released" to bind to the polyubiquitin-NEMO complex, thus shifting the equilibrium to the extent that further IKK activation is not allowed.

This hypothesis begs the question of how the sequestration of A20 is regulated. An intriguing hypothesis is that ITCH ubiquitin ligase activity towards this phospho-A20 binding protein would itself be regulated by JNK. JNK has been reported to phosphorylate ITCH and promote its activity (Gao et al., 2004). Thus, once JNK becomes active (resulting from TAK1 activation of MAP2K's), it would phosphorylate ITCH, activating its Ub ligase activity towards the phospho-A20 binding protein, resulting in its degradation. Thus, the signaling pathway would have an inherent mechanism to coordinate the activation and suppression of IKK, independently of new protein synthesis.

Figure 3.21

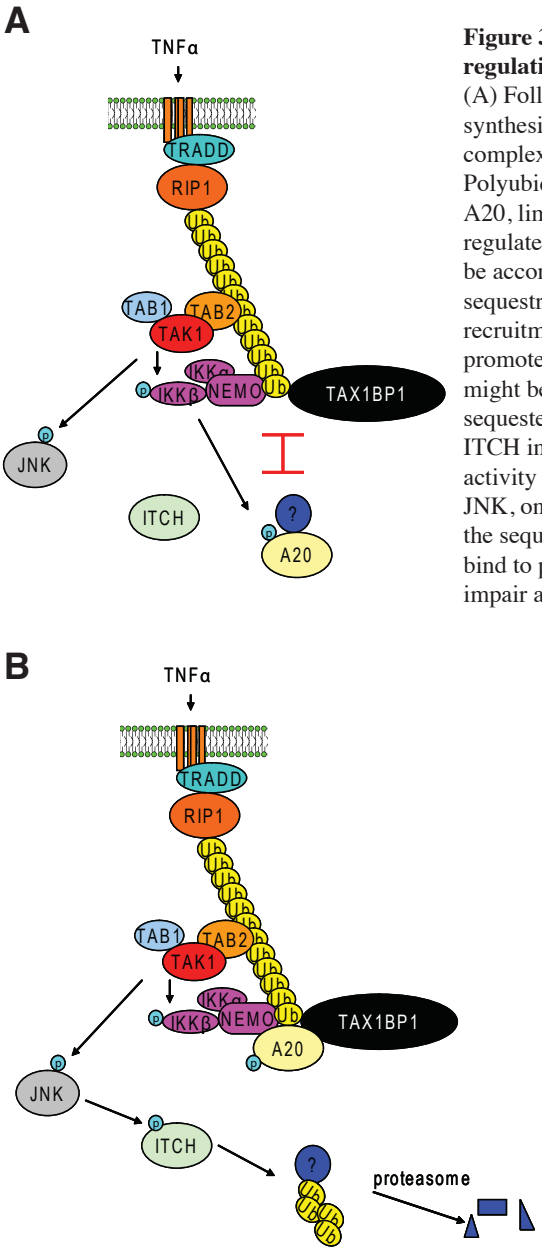

Figure 3.21. A hypothesis to explain the mechanisms of A20 regulation by IKK and E3 ubiquitin ligases.
(A) Following detection of TNFα, polyubiquitin chains are synthesized, allowing recruitment of the TAK1 and IKK complexes through ubiquitin binding by TAB2 and NEMO. Polyubiquitin chains also mediate recruitment of TAX1BP1 and A20, limiting the activaiton of IKK. However, IKK also regulates A20 function by limiting its recruitment. This might be accomplished by phosphorylating A20, leading to its sequestration by an as-yet-unidentified protein. By limiting recruitment of A20, IKK allows itself to gain activity and promote NF-κB activation. (B) This sequestration of A20 might be overcome by ubiquitination and degradation of the sequestering protein, explaining the need for the E3 ligase ITCH in recruitment of A20 and downregulation of IKK. ITCH activity itself was shown to be regulated by phosphorylation by JNK, one of the downstream effects of TAK1 activation. With the sequestering protein degraded, A20 would be liberated to bind to polyUb, TAX1BP1, and NEMO, where it can directly impair activation of IKK.

This hypothesis yields testable predictions: (1) A20 binds to a protein in a manner dependent on phosphorylation by IKK, and this protein impairs its recruitment to NEMO and/or polyubiquitin chains, (2) Inhibition of the proteasome or JNK should impair recruitment of A20 to NEMO and enhance activation of IKK.

To identify proteins that bind to A20 in an IKK-dependent manner, I took advantage of an odd phenomenon I had observed earlier with the Flag-A20 overexpression cell line. Despite the inability of these cells to activate IKK in response to TNFα (Figure 3.1A), the cells still had some activation of IKK in response to IL-1β. This may be due to the fact that this particular cell line overexpresses the IL-1R. Consistent with this hypothesis, MEFs (which express endogenous TNFR and IL-1R) overexpressing A20 did not have detectable IKK activation in response to TNFα or IL-1β (data not shown).

In any case, the HEK293 (IL-1R) cells with Flag-A20 allowed affinity purification of A20 in the absence or presence of IKK activation by IL-1β. These cells were untreated or treated with IL-1β in the absence or presence of the IKK inhibitor TPCA-1. Flag immunoprecipitation was performed, and the IP products were separated by SDS-PAGE and silver stained. Remarkably, several proteins were present following IL-1β stimulation without TPCA-1, but not when TPCA-1 was present, suggesting an IKK-dependent interaction (Figure 3.22A). These proteins were excised from the gel, digested with trypsin, and identified by mass spectrometry (Figure 3.22B). Surprisingly, the most prominent bands from the IL-1β minus TPCA-1 sample were all subunits of myosin. The most prominent band, at ~225 kDa, was non-muscle myosin heavy polypeptide 9 (MHC). Immunoblotting with an antibody against MHC confirmed that MHC co-immunoprecipitated with overexpressed A20 after IL-1β stimulation, but not when TPCA-1 was present (Figure 3.22C, lane 2). This was in contrast to NEMO, which

was only detectable in A20 immunoprecipitates after treatment of cells with both IL-1β and TPCA-1 (lane 3). To see whether endogenous MHC and A20 interact in a stimulus dependent manner, HEK293 cells were stimulated with TNFα, and immunoprecipitation of MHC followed by immunoblotting for A20 were performed. Indeed, following TNFα stimulation, A20 co-immunoprecipitated with MHC (Figure 3.22D).

Best known for its classical function as a cytoskeletal protein, little is known regarding a potential signaling role of MHC in NF-κB regulation. To see whether MHC regulates NEMO-A20 interaction and/or IKK activity, a small molecule inhibitor of MHC ATPase activity, blebbistatin was used. In S100, even at 500 μM concentration, blebbistatin had no effect on IKK activation by TRAF6 (Figure 3.23A-B). Moreover, following immunodepletion of MHC from HeLa S100, TRAF6-induced IKK activation and NEMO-A20 interaction were no different than in S100 depleted with non-specific IgG (Figure 3.23C). It should be noted that, even after three rounds of MHC immunodepletion, a small percentage of MHC remained in the S100, leaving open the possibility that MHC was still able to affect the NEMO-A20 interaction and IKK activity. However, because further depletion could not be accomplished (data not shown), and blebbistatin did not affect NEMO-A20 interaction or IKK activity, no further work on this subject was performed.

To test the hypothesis that recruitment of A20 to NEMO is dependent on the proteasome and JNK activity, HEK293 cells were treated with inhibitors of either the proteasome (MG-132) or JNK (SP600125), then the cells were stimulated with TNFα, and NEMO-A20 interaction and IKK activity were assayed. Treatment of the cells with either MG-132 or SP600125 resulted in slightly delayed recruitment of A20 to NEMO and enhanced IKK activity (Figures 3.24A-B). These results suggest that the proteasome and JNK activity do indeed play a role in recruitment

Figure 3.22

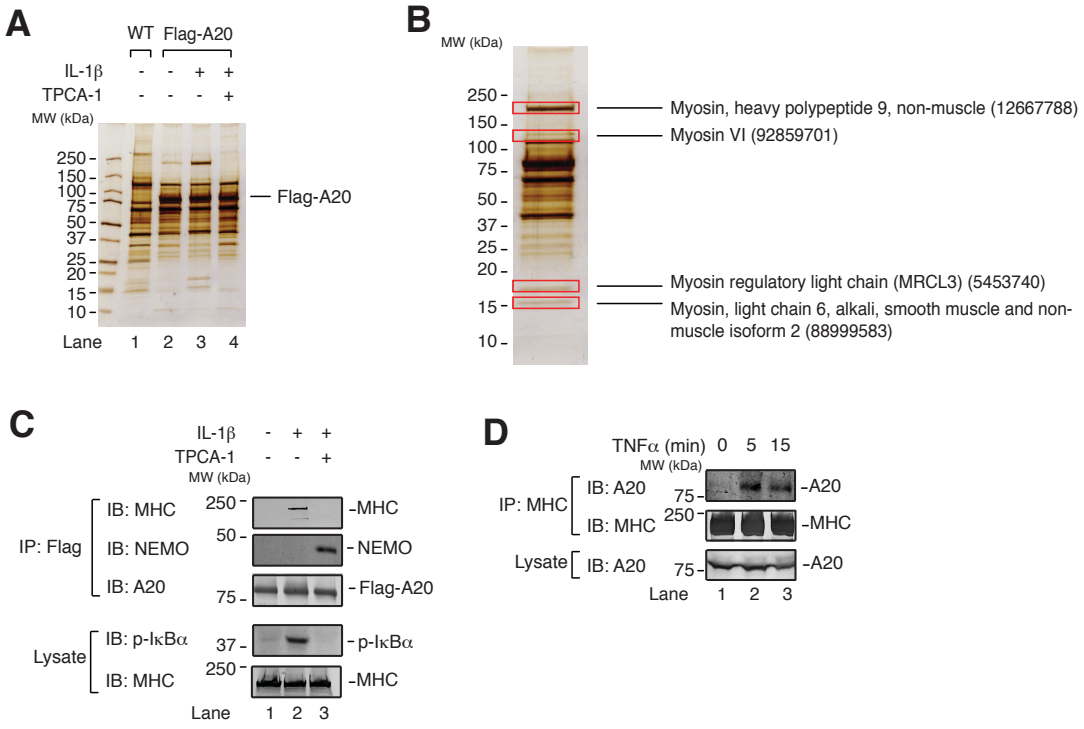

Figure 3.22. A20 interacts with non-muscle myosin heavy chain in an IKK-dependent manner. (A) HEK293 cells that express the IL-1R and Flag-A20, or parental cells (WT) as a control, were treated with TPCA-1 (10 μM) or DMSO for 3 hr. Cells were then untreated or treated with IL-1β for 10 min. Lysates were used for immunoprecipitation with anti-Flag sepharose, followed by elution with Flag peptide. Eluates were run on a 4-20% gradient gel and silver stained. (B) Magnification of lane 3 from (A). Red boxes indicate bands that were excised, digested with trypsin, and analyzed by LC-MS/MS. The name of each protein is indicated, followed by its accession number in parenthesis. (C) HEK293 cells that express the IL-1R and Flag-A20 were treated with TPCA-1 (10 μM) or DMSO for 3 hr. Cells were then untreated or treated with IL-1β for 10 min. Lysates were used for immunoprecipitation with anti-Flag sepharose, followed by elution with Flag peptide. Lysates and Flag eluates were immunoblotted with the indicated antibodies. (D) HEK293 cells were treated with TNFα for the indicated times. Lysates were used for immunoprecipitation with an antibody against MHC. Lysates and immunoprecipitates were immunoblotted with the indicated antibodies.

Figure 3.23

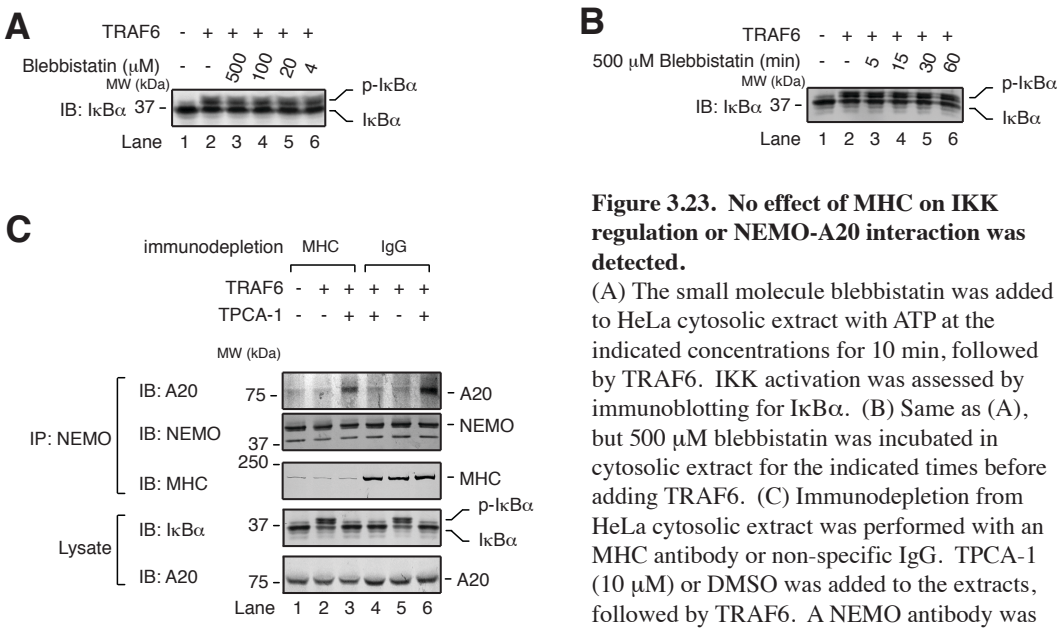

Figure 3.23. No effect of MHC on IKK regulation or NEMO-A20 interaction was detected.
(A) The small molecule blebbistatin was added to HeLa cytosolic extract with ATP at the indicated concentrations for 10 min, followed by TRAF6. IKK activation was assessed by immunoblotting for IκBα. (B) Same as (A), but 500 μM blebbistatin was incubated in cytosolic extract for the indicated times before adding TRAF6. (C) Immunodepletion from HeLa cytosolic extract was performed with an MHC antibody or non-specific IgG. TPCA-1 (10 μM) or DMSO was added to the extracts, followed by TRAF6. A NEMO antibody was used for immunoprecipitation. Extracts and immunoprecipitates were immunoblotted with the indicated antibodies.

Figure 3.24

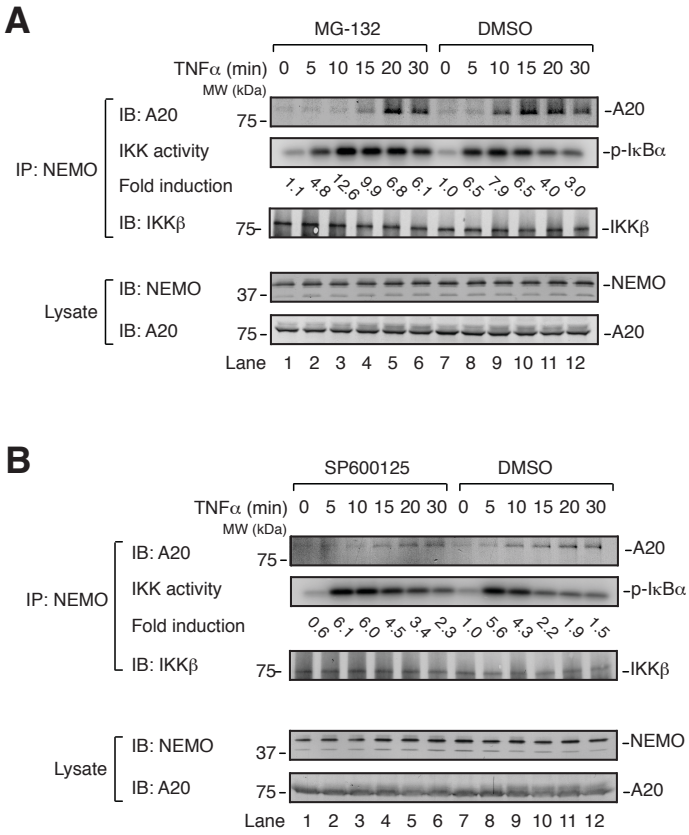

Figure 3.24. TNFα-induced NEMO-A20 interaction is delayed and IKK activity is enhanced in the presence of proteasome or JNK inhibitors. (A) HEK293 cells were treated with MG-132 (40 μM) or DMSO for 1 hr. Cells were then treated for the indicated times with TNFα. Lysates were used for immunoprecipitation with a NEMO antibody, and immunoprecipitate was used to measure IKK activity or for immunoblotting with the indicated antibodies. Fold induction indicates the density of IκBα phosphorylation relative to that in the untreated, DMSO sample (lane 7). (B) Same protocol as (A), except the JNK inhibitor SP600125 (10 μM) was used instead of MG-132.

of A20 to NEMO and negative regulation of IKK. However, because the influence of the drugs was relatively modest, and because no other IKK-dependent A20-interacting proteins could be identified, this idea was not pursued further.

Materials and Methods

Stimulation of cells and analyses by immunoblotting, immunoprecipitation, and kinase assays

HEK293 cells, HeLa cells, U2OS cells, or MEFs were treated with IL-1β (30 ng/ml) or GST-TNFα (1 ug/ml). Cells were lysed in Buffer A (20 mM Tris-HCl [pH 7.5], 150 mM NaCl, 20 mM β-glycerolphosphate, 1 mM DTT, 0.5% NP-40, and Complete protease inhibitor cocktail [Roche]). Cell lysates were centrifuged at 20,000 x g for 10-15 min, and supernatant was used for immunblotting or immunoprecipitation according to standard protocols.

For IKK activity assays, following immunoprecipitation of NEMO and several washes in Buffer A, immunoprecipitate was washed with Buffer B (20 mM Tris-HCl [pH 7.5], 1 mM DTT, 20 mM β-glycerolphosphate, 0.05% NP-40). Following removal of Buffer B, the immunoprecipitate was incubated with GST-IκBα N-terminus (0.1 mg/ml), 10 μM ATP, and γ-^{32}P-ATP at 30° for 30 min.

For TAK1 activity assays, the protocol was the same, except a TAB2 antibody was used for immunoprecipitation, and His_6-MKK6 (K82A) was used as a substrate.

Cell-free assays of IKK activity

HeLa S100 was prepared according to standard protocols. S100 was mixed with 5X Buffer C (100 mM Tris-HCl [pH 7.5], 2.5 mM DTT, 100 mM β-glycerophosphate, 12.5 mM ATP, and 25 mM $MgCl_2$) for a final concentration of 1X buffer C and 1.2 μg of total protein per 1 μl. Flag-purified A20 was added as indicated, then His_6-TRAF6 was added to ~100 nM final. After 30 min at 30°, reaction was analyzed by IκBα immunoblot or IKK activity assay as indicated.

For assays with purified TAK1 and IKK complexes, IKK complex was used at ~5 nM, TAK1 complex at ~1 nM, MKK6 (K82A) at ~1 μM, and two-step affinity-purified A20 at ~3-100 nM. Synthesis and purification of polyubiquitin chains, as well as purification of TAK1 and IKK complexes, were described previously (Xia et al., 2009). Components were mixed with Buffer C. After 30 min at 30°, reaction was analyzed by immunoblotting as indicated.

Generation of constitutively active TAK1 (TAK1-ca)

TAK1 complex (~1 nM) was mixed with ubiquitination enzymes as described (Xia et al., 2009), for 30 min. K63R ubiquitin (Boston Biochem) was added to 25 μM, and viral OTU was added to ~3 μM, and reaction was incubated at room temperature for 30 min. Reaction was diluted 1:2 in Buffer D (20 mM Tris-HCl [pH 7.5], 150 mM NaCl, 1 mM DTT, 0.5% NP-40), and M2 beads were added. Sample was rotated end-over-end overnight at 4°. Beads were rinsed in Buffer D, then Buffer E (20 mM Tris-HCl [pH 7.5], 50 mM NaCl, 1 mM DTT, 0.05% NP-40, 5% glycerol). TAK1 complex was eluted with 0.2 mg/ml Flag peptide.

A20-polyubiquitin binding assays

Constructs encoding N-terminally Flag-tagged A20, or mutants thereof, were transfected into HEK293 cells by $CaPO_4$ precipitation. Cells were lysed in Buffer D, and 20,000 x g supernatant was incubated for 4-6 hr with M2 (anti-Flag) agarose. Beads were washed with Buffer D, then with Buffer E. Protein was eluted with 0.2 mg/ml Flag peptide. This partially purified A20 was mixed with polyubiquitin chains synthesized by E1, UBC13/UEV1A, and TRAF6, in which some of the ubiquitin had an HA tag (Boston Biochem), in Buffer F (20 mM Tris-HCl [pH 7.5], 100 mM NaCl, 0.5 mM DTT, 0.2% NP-40, 5% glycerol, 0.1 mg/ml BSA) on ice for 15 min. 10% of reaction was analyzed by immunoblotting for HA. Remaining reaction was diluted 1:10 in Buffer F, then mixed with M2 sepharose. Beads were rinsed with Buffer G (Buffer F without BSA), then with Buffer E. A20 was eluted with 0.2 mg/ml Flag peptide. Eluate was analyzed by immunoblotting for HA and Flag.

Rescue of A20 function in $A20^{-/-}$ MEFs with retrovirus

Constructs and protocol for preparation of retrovirus to express A20 were described previously (He and Ting, 2002). A20 mutants were subcloned into retroviral expression vector by PCR using standard methods. $A20^{+/+}$ and $A20^{-/-}$ MEFs were prepared from the wild-type and mutant mice and immortalized with SV40 large T antigen. These cells were infected with retrovirus in the presence of polybrene (1.7 μg/ml final). 6 hr later, virus media was replaced with fresh media. 24 hr later (30 hr after infection), cells were stimulated as indicated and harvested. 20,000 x g supernatant was analyzed for A20 expression using a polyclonal antibody that can recognize both human and mouse A20 (Boone et al., 2004). Remaining supernatant was used for NEMO immunoprecipitation-IKK assay. Kinase activity was quantitated using ImageQuant software (Molecular Dynamics).

Generation of stable cell lines using Lentivirus

Lentiviral vector and associated plasmids for generation of virus were provided by Dr. Yi Zhang (University of North Carolina at Chapel Hill). Virus expressing GFP or A20 was prepared as described in (He et al., 2011). $A20^{+/+}$ or $A20^{-/-}$ MEFs were infected with lentivirus in the presence of polybrene (1.7 μg/ml final). 24 hr later, puromycin was added to 1 μg/ml final. After selection, pools of cells with stable expression were used for further analysis.

RT-PCR measurements of NF-κB target gene expression

RNA was extracted using Trizol, then Chloroform using standard protocols. The iScript cDNA synthesis kit (BioRad) was used to create cDNA from 150 ng of RNA. Quantitative real time PCR was performed using Sybr® Green on a BioRad iCycler iQ™5 with the following primers: rp119 (AAATCGCCAATGCCAACTC; TCTTCCCTATGCCCATATGC); IL-6 (TCCATCCAGTTGCCTTCTTG; GGTCTGTTGGGAGTGGTATC); COX-2 (TCC TCA CAT CCC TGA GAA CC; AAG TGG TAA CCG CTC AGG TG). rp119 values were used as a standard for IL-6 and COX-2 values. Data were normalized to unstimulated WT MEFs.

Direct binding between NEMO, polyubiquitin chains, and A20

GST or GST-NEMO (~20 nM), two-step affinity-purified A20 (~10-120 nM) and purified K63 polyubiquitin chains (~25 nM assuming average molecular weight of 400 kDa) were mixed on ice for 15 min in Buffer F. 10% of the reaction was analyzed by immunoblotting as indicated. Remaining reaction was diluted 10-fold in Buffer F. Glutathione Sepharose 4B

(GE Healthcare) was added and samples were rotated end-over-end at 4° for 1 hr. Beads were washed several times in Buffer G, then analyzed by immunoblotting as indicated.

Protein phosphatase and deubiquitination treatment of IKK complex

HEK293 cells were unstimulated or stimulated for 10 min with GST-TNFα. Cells were harvested in Buffer A, and 20,000 x g supernatant was incubated with anti-NEMO antibody and Protein A/G beads. Beads were washed in Buffer A, then with Buffer H (20 mM Tris-HCl [pH 7.5], 1 mM DTT, 0.05% NP-40). Beads were re-suspended in 15 μl of Buffer I (20 mM Tris-HCl [pH 7.5], 0.5 mM DTT, 0.2 mg/ml BSA), -/+ viral OTU (~ 30 μM), then incubated at 30° for 30 min. Buffer I was removed and replaced with Lambda protein phosphatase buffer (New England Biolabs) according to manufacturer's instructions, -/+ 400 U of lambda phosphatase. After 10 min at 30°, phosphatase buffer was removed, beads were rinsed with Buffer A, then with Buffer B. Kinase assay was then performed as described above.

Plasmids

Expression plasmids for E1, UBC13, UEV1A, UBC5, TRAF6, TAB2, MKK6 (K82A), MEKK1, and TAK1 were described previously (Deng et al., 2000; Lee et al., 1997; Xia et al., 2009). N-terminally Flag-tagged A20 for expression in HEK293 cells was constructed in pcDNA3.1 or pEAK. N-terminally TAP-tagged, C-terminally Flag-tagged A20 was constructed in pEF-IRES-P. Deletion and point mutagenesis were performed by PCR using standard methods. All constructs were verified by DNA sequencing. GST-NEMO ΔN was constructed in Gateway pDEST 15 (Invitrogen). The bacterial expression plasmid for the viral OTU was provided by A. Garcia-Sastre (Frias-Staheli et al., 2007).

Cell culture, antibodies, reagents

HEK293 cells were maintained in DMEM (Cellgro) supplemented with 10% calf serum (Hyclone) and antibiotics (penicillin G [100 μg/ml) and streptomycin [10 μg/ml]). MEF cells and HeLa cells were maintained in DMEM supplemented with 10% fetal bovine serum (Hyclone) and antibiotics. U2OS cells were maintained in DMEM supplemented with 10% tetracycline-free fetal bovine serum (Hyclone) and antibiotics.

A20-overexpression cell line was prepared by infecting HEK293 cells with retrovirus expressing Flag-A20 and selecting with puromycin (1 μg/ml). Single colonies were scaled up and tested for A20 expression by immunoblotting.

Antibodies used in this study and their sources and catalog numbers are as follows: Santa Cruz Biotech: IκBα (371) Ub (8017), NEMO (8330), IKKα/β (7607), p-MKK6 (7994); Imgenex: A20 (161A); Cell Signaling: IκBα (4814), phospho-IκBα (9246), p-IKKα/β (2078), p-TAK1 (4536), TNF-R1 (3736); BD Bioscience: IKKβ (611254), RIP1 (610458), NEMO (557383), TRADD (610572); Zymed: UBC13 (37-1100); Covance: GST (MMS-112P), HA (MMS-101P); Sigma: Flag (F3165 and F4042); Qiagen: penta-His (34660). For detection of mouse A20, a homemade antibody was used(Boone et al., 2004).

Other commonly used reagents: M2 (anti-Flag) sepharose (Sigma A2220), A/G sepharose (Pierce #53133), Glutathione Sepharose 4B (GE Healthcare), Ni-NTA agarose (Qiagen). TPCA-1, BMS-345541, and coumermycin were purchased from Sigma and dissolved in DMSO.

Protein expression and purification

GST and GST-tagged NEMO, NEMO ΔN, IκBα 1-54 (NT), TNFα, IL-1β, and viral OTU (CCHFV-L [1-169]) were expressed in E. Coli BL21/pLys and purified using Glutathione Sepharose 4B. GST tag was removed from IL-1β and viral OTU by thrombin. E1, TRAF6, and TAB2 were expressed in Sf9 cells as His_6-tagged proteins and purified using Ni-NTA agarose. UBC13, UEV1A, UBC5, MKK6 (K82A), and TEV protease were expressed in E. Coli BL21/pLys as His_6-tagged proteins and purified using Ni-NTA agarose.

To purify the IKK complex, $NEMO^{-/-}$ MEF cells and $NEMO^{-/-}$ MEF cells reconstituted with Flag-NEMO were harvested in Buffer C. 20,000 x g supernatants were mixed at a 10:1 ratio for 30 min, then mixed with M2 agarose overnight. Beads were rinsed with Buffer C, then Buffer F. IKK complex containing Flag-NEMO was eluted with 0.2 mg/ml Flag peptide.
NOTE: This purification was performed by Jueqi Chen.

Pull-down of TNFR

For "0" timepoint, A20-overexpression or parental cells were cooled to 4°, then treated with GST-TNFα for 10 min. For 5' and 15' timepoints, cells that were not cooled were treated with GST-TNFα as indicated. Cells were harvested in Buffer A, then centrifuged at 20,000 x g for 15 min. Supernatant was mixed with glutathione sepharose 4B. Beads were washed with Buffer A, then analyzed by immunoblotting as indicated.

Mass spectrometry

Following separation by SDS-PAGE and silver staining, protein bands were manually excised, de-stained, and digested with trypsin at 37° for 16 hr using standard protocols. Tryptic peptides were extracted in 50% acetonitrile (ACN), 5% Formic acid (FA), then lyophilized to

near dryness. Samples were resuspended in 10 μl of 2% ACN, 0.1% FA. 1-5 ml of sample was loaded via an autosampler (Finnigan Micro AS) onto a trap column (New Objective; 5 μm PROTEOPEP^{TM} II C18, 300 Å, 100 μm x 25 mm) using an HPLC system (Eksigent NanoLC 2D) at 5 μl/min for 2.6 min in 2% ACN, 0.1% FA. Peptides were eluted from the trap column and directly separated on an analytical column with an electrospray tip packed in house (Michrom, 3 μm Magic C18, 100Å; 76 μm x 105 mm) at a flow rate of 200 nL/min. A 60 min gradient of solution A (water + 0.1% FA) and solution B (100% ACN + 0.1% FA) was used according to the following program: 2% B, 0-5 min; 2-40% B, 5-40 min; 40% B, 40-45 min; 80% B, 45-55 min; 2% B, 55-60 min. Eluted peptide ions were scanned by an LTQ XL mass spectrometer (Thermo) with a spray voltage of 2 kV. MS/MS spectra were acquired in data-dependent mode with dynamic exclusion whereby the six most abundant parent ions were subjected to further fragmentation by collision-induced association (CID). The spectra were used to search the human RefSeq protein database using Sequest (Thermo) software.

Depletion of UBC13 from S100

His_6-tagged UEV1A was coupled to NHS-activated sepharose 4 Fast Flow (GE Healthcare) according to manufacturer's instructions. Sepharose was incubated with HeLa S100 (~1 mg of UEV1A per 3 mg total protein) three times, rotating end-over-end at 4° for 4 hr or overnight. The third flow-through was used for assays.

Negative-stain electron microscopy

1-2 μl of TAK1 complex was loaded on freshly glow-discharged carbon-coated copper grids and stained with 6% ammonium molybdate at pH 6.8 + 0.1% trehalose. The grids were

examined using a Tecnai G2 Spirit BioTWIN transmission electron microscope (TEM). Images of stained complexes were tanken with a CCD camera with a defocus level varying from -0.9 to -2.5 μm. >5,000 particles were picked manually using BOXER software.

Immunofluorescence microscopy

Cells were grown on coverslips in 24-well plates. Following the indicated treatments with coumermycin or IL-1β, cells were rinsed with PBS, then fixed in 3.7% formaldehyde in PBS for 15 min. Cells were permeabilized and blocked for 30 min at room temperature in a staining buffer containing 0.2% Triton-X and 3% BSA in PBS. Cells were next incubated with primary antibody in staining buffer for 45 min at room temperature. After washing three times in PBS with 0.2% Triton-X, cells were incubated with secondary antibody in staining buffer for 45 min at room temperature. After rinsing three times with PBS, the coverslips were briefly dipped in water, the mounted onto slides using mounting media (VectaShield; Vector Laboratories). Imaging was carried out using Zeiss LSM510 META laser scanning confocal microscopy.

Bibliography

Bagneris, C., Ageichik, A.V., Cronin, N., Wallace, B., Collins, M., Boshoff, C., Waksman, G., and Barrett, T. (2008). Crystal structure of a vFlip-IKKgamma complex: insights into viral activation of the IKK signalosome. Mol Cell *30*, 620-631.

Baud, V., and Karin, M. (2009). Is NF-kappaB a good target for cancer therapy? Hopes and pitfalls. Nat Rev Drug Discov *8*, 33-40.

Bianchi, K., and Meier, P. (2009). A tangled web of ubiquitin chains: breaking news in TNF-R1 signaling. Mol Cell *36*, 736-742.

Bignell, G.R., Warren, W., Seal, S., Takahashi, M., Rapley, E., Barfoot, R., Green, H., Brown, C., Biggs, P.J., Lakhani, S.R.*, et al.* (2000). Identification of the familial cylindromatosis tumour-suppressor gene. Nat Genet *25*, 160-165.

Boone, D.L., Turer, E.E., Lee, E.G., Ahmad, R.C., Wheeler, M.T., Tsui, C., Hurley, P., Chien, M., Chai, S., Hitotsumatsu, O.*, et al.* (2004). The ubiquitin-modifying enzyme A20 is required for termination of Toll-like receptor responses. Nat Immunol *5*, 1052-1060.

Bosanac, I., Wertz, I.E., Pan, B., Yu, C., Kusam, S., Lam, C., Phu, L., Phung, Q., Maurer, B., Arnott, D.*, et al.* (2010) Ubiquitin Binding to A20 ZnF4 Is Required for Modulation of NF-kappaB Signaling. Mol Cell *40*, 548-557.

Chen, Z.J., and Sun, L.J. (2009). Nonproteolytic functions of ubiquitin in cell signaling. Mol Cell *33*, 275-286.

Compagno, M., Lim, W.K., Grunn, A., Nandula, S.V., Brahmachary, M., Shen, Q., Bertoni, F., Ponzoni, M., Scandurra, M., Califano, A.*, et al.* (2009). Mutations of multiple genes cause deregulation of NF-kappaB in diffuse large B-cell lymphoma. Nature *459*, 717-721.

De Valck, D., Jin, D.Y., Heyninck, K., Van de Craen, M., Contreras, R., Fiers, W., Jeang, K.T., and Beyaert, R. (1999). The zinc finger protein A20 interacts with a novel anti-apoptotic protein which is cleaved by specific caspases. Oncogene *18*, 4182-4190.

Deng, L., Wang, C., Spencer, E., Yang, L., Braun, A., You, J., Slaughter, C., Pickart, C., and Chen, Z.J. (2000). Activation of the IkappaB kinase complex by TRAF6 requires a dimeric ubiquitin-conjugating enzyme complex and a unique polyubiquitin chain. Cell *103*, 351-361.

Ea, C.K., Deng, L., Xia, Z.P., Pineda, G., and Chen, Z.J. (2006). Activation of IKK by TNFalpha requires site-specific ubiquitination of RIP1 and polyubiquitin binding by NEMO. Mol Cell *22*, 245-257.

Evans, P.C., Ovaa, H., Hamon, M., Kilshaw, P.J., Hamm, S., Bauer, S., Ploegh, H.L., and Smith, T.S. (2004). Zinc-finger protein A20, a regulator of inflammation and cell survival, has de-ubiquitinating activity. Biochem J *378*, 727-734.

Farrar, M.A., Alberol-Ila, J., and Perlmutter, R.M. (1996). Activation of the Raf-1 kinase cascade by coumermycin-induced dimerization. Nature *383*, 178-181.

Field, N., Low, W., Daniels, M., Howell, S., Daviet, L., Boshoff, C., and Collins, M. (2003). KSHV vFLIP binds to IKK-gamma to activate IKK. J Cell Sci *116*, 3721-3728.

Frias-Staheli, N., Giannakopoulos, N.V., Kikkert, M., Taylor, S.L., Bridgen, A., Paragas, J., Richt, J.A., Rowland, R.R., Schmaljohn, C.S., Lenschow, D.J*., et al.* (2007). Ovarian tumor domain-containing viral proteases evade ubiquitin- and ISG15-dependent innate immune responses. Cell Host Microbe *2*, 404-416.

Fu, D.X., Kuo, Y.L., Liu, B.Y., Jeang, K.T., and Giam, C.Z. (2003). Human T-lymphotropic virus type I tax activates I-kappa B kinase by inhibiting I-kappa B kinase-associated serine/threonine protein phosphatase 2A. J Biol Chem *278*, 1487-1493.

Gao, M., Labuda, T., Xia, Y., Gallagher, E., Fang, D., Liu, Y.C., and Karin, M. (2004). Jun turnover is controlled through JNK-dependent phosphorylation of the E3 ligase Itch. Science *306*, 271-275.

Haas, T.L., Emmerich, C.H., Gerlach, B., Schmukle, A.C., Cordier, S.M., Rieser, E., Feltham, R., Vince, J., Warnken, U., Wenger, T*., et al.* (2009). Recruitment of the linear ubiquitin chain assembly complex stabilizes the TNF-R1 signaling complex and is required for TNF-mediated gene induction. Mol Cell *36*, 831-844.

Hayden, M.S., and Ghosh, S. (2008). Shared principles in NF-kappaB signaling. Cell *132*, 344-362.

He, J., Nguyen, A.T., and Zhang, Y. (2011) KDM2b/JHDM1b, an H3K36me2-specific demethylase, is required for initiation and maintenance of acute myeloid leukemia. Blood *117*, 3869-3880.

He, K.L., and Ting, A.T. (2002). A20 inhibits tumor necrosis factor (TNF) alpha-induced apoptosis by disrupting recruitment of TRADD and RIP to the TNF receptor 1 complex in Jurkat T cells. Mol Cell Biol *22*, 6034-6045.

Hong, S., Wang, L.C., Gao, X., Kuo, Y.L., Liu, B., Merling, R., Kung, H.J., Shih, H.M., and Giam, C.Z. (2007). Heptad repeats regulate protein phosphatase 2a recruitment to I-kappaB kinase gamma/NF-kappaB essential modulator and are targeted by human T-lymphotropic virus type 1 tax. J Biol Chem *282*, 12119-12126.

Hutti, J.E., Turk, B.E., Asara, J.M., Ma, A., Cantley, L.C., and Abbott, D.W. (2007). IkappaB kinase beta phosphorylates the K63 deubiquitinase A20 to cause feedback inhibition of the NF-kappaB pathway. Mol Cell Biol *27*, 7451-7461.

Iha, H., Peloponese, J.M., Verstrepen, L., Zapart, G., Ikeda, F., Smith, C.D., Starost, M.F., Yedavalli, V., Heyninck, K., Dikic, I.*, et al.* (2008). Inflammatory cardiac valvulitis in TAX1BP1-deficient mice through selective NF-kappaB activation. EMBO J *27*, 629-641.

Jin, D.Y., Teramoto, H., Giam, C.Z., Chun, R.F., Gutkind, J.S., and Jeang, K.T. (1997). A human suppressor of c-Jun N-terminal kinase 1 activation by tumor necrosis factor alpha. J Biol Chem *272*, 25816-25823.

Kanayama, A., Seth, R.B., Sun, L., Ea, C.K., Hong, M., Shaito, A., Chiu, Y.H., Deng, L., and Chen, Z.J. (2004). TAB2 and TAB3 activate the NF-kappaB pathway through binding to polyubiquitin chains. Mol Cell *15*, 535-548.

Kang, Y., Chen, X., Lary, J.W., Cole, J.L., and Walters, K.J. (2007). Defining how ubiquitin receptors hHR23a and S5a bind polyubiquitin. J Mol Biol *369*, 168-176.

Kato, M., Sanada, M., Kato, I., Sato, Y., Takita, J., Takeuchi, K., Niwa, A., Chen, Y., Nakazaki, K., Nomoto, J.*, et al.* (2009). Frequent inactivation of A20 in B-cell lymphomas. Nature *459*, 712-716.

Komander, D., and Barford, D. (2008). Structure of the A20 OTU domain and mechanistic insights into deubiquitination. Biochem J *409*, 77-85.

Lamothe, B., Campos, A.D., Webster, W.K., Gopinathan, A., Hur, L., and Darnay, B.G. (2008). The RING domain and first zinc finger of TRAF6 coordinate signaling by interleukin-1, lipopolysaccharide, and RANKL. J Biol Chem *283*, 24871-24880.

Laplantine, E., Fontan, E., Chiaravalli, J., Lopez, T., Lakisic, G., Veron, M., Agou, F., and Israel, A. (2009). NEMO specifically recognizes K63-linked poly-ubiquitin chains through a new bipartite ubiquitin-binding domain. EMBO J *28*, 2885-2895.

Lee, E.G., Boone, D.L., Chai, S., Libby, S.L., Chien, M., Lodolce, J.P., and Ma, A. (2000). Failure to regulate TNF-induced NF-kappaB and cell death responses in A20-deficient mice. Science *289*, 2350-2354.

Lee, F.S., Hagler, J., Chen, Z.J., and Maniatis, T. (1997). Activation of the IkappaB alpha kinase complex by MEKK1, a kinase of the JNK pathway. Cell *88*, 213-222.

Lee, S., Tsai, Y.C., Mattera, R., Smith, W.J., Kostelansky, M.S., Weissman, A.M., Bonifacino, J.S., and Hurley, J.H. (2006). Structural basis for ubiquitin recognition and autoubiquitination by Rabex-5. Nat Struct Mol Biol *13*, 264-271.

Li, L., Soetandyo, N., Wang, Q., and Ye, Y. (2009). The zinc finger protein A20 targets TRAF2 to the lysosomes for degradation. Biochim Biophys Acta *1793*, 346-353.

Lin, S.C., Chung, J.Y., Lamothe, B., Rajashankar, K., Lu, M., Lo, Y.C., Lam, A.Y., Darnay, B.G., and Wu, H. (2008). Molecular basis for the unique deubiquitinating activity of the NF-kappaB inhibitor A20. J Mol Biol *376*, 526-540.

Ling, L., and Goeddel, D.V. (2000). T6BP, a TRAF6-interacting protein involved in IL-1 signaling. Proc Natl Acad Sci U S A *97*, 9567-9572.

Massoumi, R., Chmielarska, K., Hennecke, K., Pfeifer, A., and Fassler, R. (2006). Cyld inhibits tumor cell proliferation by blocking Bcl-3-dependent NF-kappaB signaling. Cell *125*, 665-677.

Mattera, R., Tsai, Y.C., Weissman, A.M., and Bonifacino, J.S. (2006). The Rab5 guanine nucleotide exchange factor Rabex-5 binds ubiquitin (Ub) and functions as a Ub ligase through an atypical Ub-interacting motif and a zinc finger domain. J Biol Chem *281*, 6874-6883.

Musone, S.L., Taylor, K.E., Lu, T.T., Nititham, J., Ferreira, R.C., Ortmann, W., Shifrin, N., Petri, M.A., Ilyas Kamboh, M., Manzi, S.*, et al.* (2008). Multiple polymorphisms in the TNFAIP3 region are independently associated with systemic lupus erythematosus. Nat Genet.

Penengo, L., Mapelli, M., Murachelli, A.G., Confalonieri, S., Magri, L., Musacchio, A., Di Fiore, P.P., Polo, S., and Schneider, T.R. (2006). Crystal structure of the ubiquitin binding domains of rabex-5 reveals two modes of interaction with ubiquitin. Cell *124*, 1183-1195.

Poyet, J.L., Srinivasula, S.M., Lin, J.H., Fernandes-Alnemri, T., Yamaoka, S., Tsichlis, P.N., and Alnemri, E.S. (2000). Activation of the Ikappa B kinases by RIP via IKKgamma /NEMO-mediated oligomerization. J Biol Chem *275*, 37966-37977.

Reyes-Turcu, F.E., Horton, J.R., Mullally, J.E., Heroux, A., Cheng, X., and Wilkinson, K.D. (2006). The ubiquitin binding domain ZnF UBP recognizes the C-terminal diglycine motif of unanchored ubiquitin. Cell *124*, 1197-1208.

Schmitz, R., Hansmann, M.L., Bohle, V., Martin-Subero, J.I., Hartmann, S., Mechtersheimer, G., Klapper, W., Vater, I., Giefing, M., Gesk, S.*, et al.* (2009). TNFAIP3 (A20) is a tumor suppressor gene in Hodgkin lymphoma and primary mediastinal B cell lymphoma. J Exp Med *206*, 981-989.

Shembade, N., Harhaj, N.S., Liebl, D.J., and Harhaj, E.W. (2007). Essential role for TAX1BP1 in the termination of TNF-alpha-, IL-1- and LPS-mediated NF-kappaB and JNK signaling. EMBO J *26*, 3910-3922.

Shembade, N., Harhaj, N.S., Parvatiyar, K., Copeland, N.G., Jenkins, N.A., Matesic, L.E., and Harhaj, E.W. (2008). The E3 ligase Itch negatively regulates inflammatory signaling pathways by controlling the function of the ubiquitin-editing enzyme A20. Nat Immunol *9*, 254-262.

Shembade, N., Ma, A., and Harhaj, E.W. (2010) Inhibition of NF-kappaB signaling by A20 through disruption of ubiquitin enzyme complexes. Science *327*, 1135-1139.

Shembade, N., Parvatiyar, K., Harhaj, N.S., and Harhaj, E.W. (2009). The ubiquitin-editing enzyme A20 requires RNF11 to downregulate NF-kappaB signalling. EMBO J *28*, 513-522.

Song, H.Y., Rothe, M., and Goeddel, D.V. (1996). The tumor necrosis factor-inducible zinc finger protein A20 interacts with TRAF1/TRAF2 and inhibits NF-kappaB activation. Proc Natl Acad Sci U S A *93*, 6721-6725.

Sun, S.C. (2008). Deubiquitylation and regulation of the immune response. Nat Rev Immunol *8*, 501-511.

Vereecke, L., Beyaert, R., and van Loo, G. (2009). The ubiquitin-editing enzyme A20 (TNFAIP3) is a central regulator of immunopathology. Trends Immunol *30*, 383-391.

Verstrepen, L., Verhelst, K., van Loo, G., Carpentier, I., Ley, S.C., and Beyaert, R. Expression, biological activities and mechanisms of action of A20 (TNFAIP3). Biochem Pharmacol.

Wang, C., Deng, L., Hong, M., Akkaraju, G.R., Inoue, J., and Chen, Z.J. (2001). TAK1 is a ubiquitin-dependent kinase of MKK and IKK. Nature *412*, 346-351.

Wertz, I.E., O'Rourke, K.M., Zhou, H., Eby, M., Aravind, L., Seshagiri, S., Wu, P., Wiesmann, C., Baker, R., Boone, D.L.*, et al.* (2004). De-ubiquitination and ubiquitin ligase domains of A20 downregulate NF-kappaB signalling. Nature *430*, 694-699.

Wu, C.J., Conze, D.B., Li, T., Srinivasula, S.M., and Ashwell, J.D. (2006). Sensing of Lys 63-linked polyubiquitination by NEMO is a key event in NF-kappaB activation [corrected]. Nat Cell Biol *8*, 398-406.

Xia, Z.P., Sun, L., Chen, X., Pineda, G., Jiang, X., Adhikari, A., Zeng, W., and Chen, Z.J. (2009). Direct activation of protein kinases by unanchored polyubiquitin chains. Nature *461*, 114-119.

Xu, M., Skaug, B., Zeng, W., and Chen, Z.J. (2009). A ubiquitin replacement strategy in human cells reveals distinct mechanisms of IKK activation by TNFalpha and IL-1beta. Mol Cell *36*, 302-314.

Zhang, J., Stirling, B., Temmerman, S.T., Ma, C.A., Fuss, I.J., Derry, J.M., and Jain, A. (2006). Impaired regulation of NF-kappaB and increased susceptibility to colitis-associated tumorigenesis in CYLD-deficient mice. J Clin Invest *116*, 3042-3049.

Zhang, S.Q., Kovalenko, A., Cantarella, G., and Wallach, D. (2000). Recruitment of the IKK signalosome to the p55 TNF receptor: RIP and A20 bind to NEMO (IKKgamma) upon receptor stimulation. Immunity *12*, 301-311.